

A Novel Small Molecule Inhibitor of p38[?] MAP Kinase Augments Cardiomyocyte Cell Cycle Entry in Response to Direct Cell Cycle Stimulation

Riham Abouleisa¹, Jessica Miller², Ahmed Gebreil², Abou Bakr Salama², Marc Dwenger¹, Hania Abdelhafez¹, Reham Wahid¹, Adeniyi Adewumi³, Mahmoud E. Soliman³, Nader Abo-Dya⁴, and Tamer Mohamed¹

¹University of Louisville Department of Medicine

²University of Louisville School of Medicine

³University of KwaZulu-Natal College of Health Sciences

⁴University of Tabouk

February 9, 2023

Abstract

Background and Purpose: Myocardial infarction (MI) is the leading cause of mortality globally due in part to the limited ability of cardiomyocytes (CMs) to regenerate. Recently, we demonstrated that overexpression of 4 cell cycle factors, CDK1, CDK4, cyclin B1, and cyclin D1 (4F), induced cell division in ~20% of the post-mitotic CMs overexpressed 4F. The current study aims to identify a small molecule that augments 4F-induced CM cycle induction. **Experimental Approach, Key Results:** Screening of small molecules with a potential to augment 4F-induced cell-cycle induction in 60-day-old mature human induced pluripotent cardiomyocytes (hiPS-CMs) revealed N-(4,6-Dimethylpyridin-2-yl)-4-(pyridin-4-yl)piperazine-1-carbothioamide (NDPPC), which activates cell cycle progression in 4F-transduced hiPS-CMs. Autodock tool and Autodock vina computational methods showed that NDPPC has a potential interaction with the binding site at the human p38[?] mitogen-activated protein kinase (p38[?] MAP kinase), a critical negative regulator of the mammalian cell cycle. A p38[?] MAP kinase activity assay showed that NDPPC inhibits its activity in a dose-dependent manner. Overexpression of p38[?] MAP kinase in CMs inhibited 4F cell cycle induction, and treatment with NDPPC reversed the cell cycle inhibitory effect. **Conclusion and Implications:** NDPPC is a novel inhibitor for p38[?] MAP kinase and is a promising drug to augment CM cell cycle response to the 4F. NDPPC could become an adjunct treatment with other cell cycle activators for heart failure treatment.

Title: A Novel Small Molecule Inhibitor of p38 α MAP Kinase Augments Cardiomyocyte Cell Cycle Entry in Response to Direct Cell Cycle Stimulation

Short Running title: NDPPC, a novel p38 α MAP Kinase inhibitor

Riham R E Abouleisa¹, Jessica M. Miller¹, Ahmad Gebreil¹, Abou Bakr M. Salama^{1,2}, Marc Dwenger¹, Hania Abdelhafez¹, Reham M. Wahid^{1,3}, Adeniyi T. Adewumi⁴, Mahmoud E.S. Soliman⁴, Nader E. Abo-Dya^{5,6}, Tamer M A Mohamed¹.

¹ Institute of Molecular Cardiology, Division of Cardiovascular Medicine, Department of Medicine, University of Louisville, Louisville, KY

² Department of Cardiovascular Medicine, Faculty of Medicine, Zagazig University, Egypt

³ Physiology Department, Faculty of Medicine, Zagazig University, Egypt

⁴ Molecular Bio-computation and Drug Design Laboratory, School of Health Sciences, University of KwaZulu-Natal, Westville Campus, Durban 4001, South Africa

⁵ Department of Pharmaceutical Chemistry, Faculty of Pharmacy, University of Tabuk, Tabuk 71491, Saudi Arabia

⁶ Department of Pharmaceutical Organic Chemistry, Faculty of Pharmacy, Zagazig University, Zagazig 44519, Egypt

Correspondence: Tamer Mohamed (Tamer.mohamed@louisville.edu) and Nader E. Abo-Dya (nabodya@ut.edu.sa)

Authors emails

Riham R E Abouleisa (riham.abouleisa@louisville.edu), Jessica M. Miller (jessica.miller.3@louisville.edu), Ahmad Gebreil (ahmed.gibreil@louisville.edu), Abou Bakr M. Salama (aboubakr.salama@louisville.edu), Marc Dwenger (marc.dwenger@louisville.edu), Hania Abdelhafez (hania.abdelhafez@louisville.edu), Reham M. Wahid (dr_rehamwahid@yahoo.com), Adeniyi T. Adewumi (jesutomisin0707@gmail.com), Mahmoud E.S. Soliman (soliman@ukzn.ac.za),

Author Contributions:

Conceptualization: Riham R. E Abouleisa, Tamer M A Mohamed, and Nader E. Abo-Dya. **Molecular biology methodology and data analysis:** Riham R E Abouleisa, Ahmed Geibril, Jessica M. Miller, Aboubakr Salama, Marc Dwenger, Hania Abdelhafez, Reham Wahid. **Organic chemistry methodology and target prediction:** Adeniyi T. Adewumi, Nader E. Abo-Dya, and Mahmoud E.S. Soliman. **Writing—original draft preparation:** Riham R E Abouleisa. **Writing—review, and editing:** Ahmed Geibril,

Jessica M. Miller, Aboubakr Salama, Marc Dwenger, Hania Abdelhafez, Reham Wahid, Adeniyi T. Adewumi and Mahmoud E.S. Soliman. **Supervision:** Tamer M A Mohamed, and Nader E. Abo-Dya. All authors have read and agreed on this version of the manuscript.

Funding:

This research was funded by NIH grants F32HL149140 (R.R.E.A.), R01HL147921 (T.M.A.M.), P30GM127607 (T.M.A.M.), and American Heart Association grant 16SDG29950012 (T.M.A.M)

Acknowledgments:

- Dr. Bradford G. Hill, Center for Cardiometabolic Science, Christina Lee Brown Envirome Institute, Division of Environmental Medicine, Department of Medicine, University of Louisville, Louisville, KY, for providing the NDPPC and the NCT-503 compounds.
- The Centre for High-Performance Computing (CHPC), University of Cape Town, for providing the computational facilities in this study.

Conflict of Interest: Dr. Mohamed holds equities in Tenaya Therapeutics. The other authors report no disclosures.

Data availability statement: The raw data that support the findings of this study, such as the in silico target prediction, are available from the corresponding author, [T.M.A.M, and N.E.A], upon request.

Ethics approval statement: Not applicable

Permission to reproduce material from other sources: not applicable

Word count 2855 words

Bullet point summary:

What is already known

- Cardiomyocytes have limited proliferation capacity.
- p38 α MAP kinase is a critical negative regulator of the mammalian cell cycle.

What this study adds

- NDPPC is a novel inhibitor of the p38 α MAP kinase
- NDPPC primes CMs to enter the cell cycle in response to cell cycle stimulation.

Clinical significance

- NDPPC is a promising drug to augment CM cell cycle response.
- NDPPC would have future applications as a therapeutic drug for heart failure.

Abstract

Background and Purpose: Myocardial infarction (MI) is the leading cause of mortality globally due in part to the limited ability of cardiomyocytes (CMs) to regenerate. Recently, we demonstrated that overexpression of 4 cell cycle factors, CDK1, CDK4, cyclin B1, and cyclin D1 (4F), induced cell division in ~20% of the post-mitotic CMs overexpressed 4F. The current study aims to identify a small molecule that augments 4F-induced CM cycle induction.

Experimental Approach, Key Results: Screening of small molecules with a potential to augment 4F-induced cell-cycle induction in 60-day-old mature human induced pluripotent cardiomyocytes (hiPS-CMs) revealed N-(4,6-Dimethylpyridin-2-yl)-4-(pyridin-4-yl)piperazine-1-carbothioamide (NDPPC), which activates cell cycle progression in 4F-transduced hiPS-CMs. Autodock tool and Autodock vina computational methods showed that NDPPC has a potential interaction with the binding site at the human p38 α mitogen-activated protein kinase (p38 α MAP kinase), a critical negative regulator of the mammalian cell cycle. A p38 α MAP kinase activity assay showed that NDPPC inhibits its activity in a dose-dependent manner. Overexpression of p38 α MAP kinase in CMs inhibited 4F cell cycle induction, and treatment with NDPPC reversed the cell cycle inhibitory effect.

Conclusion and Implications: NDPPC is a novel inhibitor for p38 α MAP kinase and is a promising drug to augment CM cell cycle response to the 4F. NDPPC could become an adjunct treatment with other cell cycle activators for heart failure treatment.

Keywords: heart; cell cycle; P38, cyclin, small molecule, autodock, cardiomyocyte, proliferation

1. Introduction

Myocardial infarction (MI) is one of the leading causes of heart failure. CMs lost during ischemic cardiac injury cannot be replaced due to their limited proliferative capacity, which leads to progressive heart failure (Hydbring, Malumbres, & Sicinski, 2016; Ioacara et al., 2019; Malumbres & Barbacid, 2009). Although the adult mammalian heart is recalcitrant to regeneration, recent findings indicate that stimulation of the CM cell cycle is a promising approach for inducing myocardial repair (Abouleisa et al., 2022; Johnson, Mohsin, & Houser, 2021; Salama, Gebreil, Mohamed, & Abouleisa, 2021). Our previous findings showed that overexpression of combined four cell cycle factors, CDK1, CDK4, cyclin B1, and cyclin D1 (collectively known as 4F), induced cell division in ~20% of the post-mitotic mouse, rat, and human CMs (Abouleisa et al., 2022; Mohamed et al., 2018). We also showed that during 4F-induced cell cycle induction, CMs activate several biosynthetic pathways (Abouleisa et al., 2021). To confirm our finding, we screened the effect of several small molecule activators or inhibitors of the biosynthetic pathways on the 4F-induced cell cycle (Abouleisa et al., 2021). Interestingly inhibition of phosphoglycerate dehydrogenase (PHGDH) activity, the first step in the serine biosynthesis pathway, using a small molecule (NCT503), inhibits the 4F-induced cell cycle (Abouleisa et al., 2021; Pacold et al., 2016). Interestingly, in this manuscript, we are showing that the small molecule inactive control to NCT503 drug, which does not affect PHGDH activity, N-(4,6-Dimethylpyridin-2-yl)-4-(pyridin-4-yl)piperazine-1-carbothioamide (NDPPC) (Pacold et al., 2016), augments 4F-induced cell cycle induction. However, NDPPC did not have a known target protein. In this study, we used, Autodock tool and Autodock vina software to determine the mechanism of action of NDPPC and identify its target protein (Trott & Olson, 2010). p38 α MAP kinase was identified as a possible protein target of NDPPC. p38 α MAP kinase regulates the expression of genes required for mitosis in cardiomyocytes. Activation of p38 α MAP kinase reduces BrdU incorporation (marker for G1/S) in fetal cardiomyocytes. In contrast, cardiac-specific p38 α MAPK knockout mice showed increased mitosis in neonatal and adult cardiomyocytes (Engel et al., 2005). Here, we describe how we identified NDPPC as a small molecule that can augment 4F-induced cell cycle induction through inhibition of p38 α MAP kinase.

2. Results

2.1. NDPPC primes more CMs to enter the cell cycle in response to 4F

Our recent studies showed that overexpression of combined four cell cycle factors, CDK1, CDK4, cyclin B1, and cyclin D1 (collectively known as 4F), induced cell division in ~20% of the post-mitotic mouse, rat, and human CMs (Abouleisa et al., 2021; Abouleisa et al., 2022; Mohamed et al., 2018; Salama et al., 2022). Our previous publication showed that 4F-induced cell cycle induction in CMs is associated with the activation of the biosynthetic metabolic pathways (Abouleisa et al., 2021). Therefore, we screened several drugs that inhibit or activate the biosynthetic metabolic pathways in 60-day-old mature human

induced pluripotent cardiomyocytes (hiPS-CMs) overexpressing the 4F and assessed the increase in EDU (DNA synthesis marker) and PHH3 (G2/M phase marker) (Abouleisa et al., 2021). This screening revealed a small molecule, N-(4,6-Dimethylpyridin-2-yl)-4-(pyridin-4-yl)piperazine-1-carbothioamide (NDPPC), augments the cell cycle progression in 4F-transduced hiPS-CMs as indicated by a significant increase in both PHH3 and EDU positive nuclei compared to vehicle-treated 4F-transduced hiPS-CMs (**Supplementary Figure 1**). NDPPC is the inactive control of NCT503, a small molecule inhibitor of PHGDH activity which is the rate-limiting step of the serine biosynthetic pathway (Pacold et al., 2016). This study and our previous publication showed that NCT503 reduced cell cycle induction in response to the 4F (Abouleisa et al., 2021) (**Supplementary figure 1**). To investigate the effect of NDPPC on cell cycle induction, 60-day-old mature hiPS-CMs were transfected with either 4F or LacZ (control) adenoviruses and treated with 0.1, 0.5, 1, and 5 μ M NDPPC for 48 h. As expected, 4F showed 20% of the CMs nuclei stained positive to the cell cycle markers (EDU and PHH3) compared to less than 1% in the LacZ-treated CMs. Additionally, NDPPC significantly increased PHH3 and EDU staining in 4F-treated CMs in a dose-dependent manner, with no significant increase in PHH3 nor EDU in LacZ-treated CMs (**Figure 1A, B, C**). These data suggest that the NDPPC drug enhances the ability of CMs to enter the cell cycle in response to 4F.

2.2. *In Silico* target prediction revealed that NDPPC is a potent inhibitor of p38 α MAP kinase.

To identify the target protein for the NDPPC that mediates cardiomyocyte proliferation, Autodock tool and Autodock vina software were used. First, we screened the 2D and 3D structures of NDPPC against the most prominent human cell cycle gene activators and inhibitors (Salama et al., 2021). The screening revealed that NDPPC has a binding affinity to p38 α MAP kinase similar to SB203580, a known inhibitor of p38 α MAPK (Birkenkamp et al., 2000) (**Figure 2**). SB203580 is used in this study as a reference indicator. NDPPC and NCT503 have closely related piperazine carbothioamide scaffolds and are structurally dissimilar to SB203580. The docking binding energy scores (kcal/mol) obtained from the SB203580 redocking and docking of NDPPC and NCT503 to the ATP binding site of p38 α MAP kinase are -8.3, -5.8, and -6.6, respectively. These results indicated that SB203580 bound-p38 α MAP kinase ATP site produced a significantly higher binding affinity than NDPPC and NCT503-bound p38 α MAP kinase ATP binding site. Thus, SB203580 could be more effective against p38 α MAP kinase protein at the ATP binding site than NDPPC and NCT503. NCT503 showed significantly higher binding energy than NDPPC, which is against our biological findings that NCT503 is a more potent inhibitor to PHGDH rather than p38 α MAPK compared to NDPPC. This contradictory finding could be due to the molecular docking packages' limitations, such as their bias towards the steric hindrance (Hollingsworth & Dror, 2018). Therefore, we subjected the interaction between the three compounds and the p38 α MAP kinase protein to apo (unphosphorylated p38 α MAP kinase) and five ligand-bound p38 α MAP kinase systems for

molecular dynamics (MD) simulations with the graphic processor unit (GPU) version of AMBER18, integrated CUDA engine, and LEAP modules (Case et al., 2005).

Protein-ligand interaction networks can reveal the mechanism of activation or inhibition of protein activity. The previous reports have shown that the apo, unphosphorylated p38 α MAP kinase may be used to regulate critical cellular cascades (Haar, Prabakhar, Liu, & Lepre, 2007; Wang et al., 1998; Z. Wang et al., 1997), which makes it a suitable target for this study. The SB203580, NDPPC, and NCT503 interactions with the p38 α MAP kinase ATP binding site were examined to understand their inhibitory affinity and mechanism. We investigated the interaction options between the p38 α MAP kinase binding landscape and the ligands, including the SB203580 (reference inhibitor), NDPPC, and NCT503, at the ATP binding site of the p38 α MAP kinase. SB203580 binds to the low-active or phosphorylated p38 α MAP kinase conformation to compete with ATP, indicating the p38 α MAP kinase activity inhibition. The p38 α MAP kinase-SB203580 surface residues were defined as the ATP pocket (located in the N-terminal domain) of an unphosphorylated, weak activity p38 α MAP kinase (Wang et al., 1998). Chemically, SB203580 has a core imidazole ring, a 4-fluorophenyl ring, and a pyridine ring bonded to an imidazole atom. Both NDPPC and NCT503 have a piperazine-1-carbothioamide scaffold. While NDPPC has two pyridine rings, NCT503 contains one pyridine ring.

We computed the per-residue-based energy decomposition (PRED) and obtained the energy contribution of the individual residue that interacted at the ATP binding site. The contributing residues to the binding of SB203580 and the interaction forces options are shown in **Figure 3**. The 3D interaction networks between the residues and ligands (NDPPC and NCT503) at the ATP binding site are shown in **Figures 4 and 5**, respectively. The two carbothioamide analogs interact with the active sites. The average structure obtained from a normalized 40 ns trajectory was used to compute the PRED contributions, which enables the understanding of interaction force options between the protein and ligands. The binding free energy of the ATP-bound site residues was decomposed into energy contributions.

The structure of the p38 α MAP kinase-SB203580 complex revealed many interactions, including H-bonds (classical and carbon-hydrogen), electrostatic pi-charge, mixed pi/alkyl hydrophobic, and halogen fluorine during the MD simulations. **Figure 3A** shows that the methyl sulfinyl phenyl ring of SB203580 interacted with VAL38 and LEU167 of the phosphorylation lip, while the pyridyl ring became buried in the ATP site, partly due to the interactions with activation loop residues LEU108 and MET109. **Figure 3B** illustrates the intermolecular forces between the interacting residues and the SB203580. **Figure 3C** plot displays energy contributed by each interacting residue. VAL38 (-1.565 kcal/mol), ALA51 (-1.074 kcal/mol), LYS53 (~ -1.018 kcal/mol), ILE84 (~ -1.0 kcal/mol), HIE107 (0.037 kcal/mol), LEU108 (-1.248 kcal/mol), MET109 (-1.381 kcal/mol), and LEU167 (-1.450 kcal/mol) are some of the residues that play critical roles in the regulatory activity of p38 α MAP kinase (Haar et al., 2007). However, HIE107 and LEU104 showed no significant contribution to binding with SB203580, while VAL38, LYS53, ILE84, LEU108, MET109, and LEU167 (-1.4 kcal/mol) contributed the highest binding energies to the interaction with SB203580.

VAL38, ALA51, and ILE84 simultaneously formed pi-alkyl hydrophobic interactions with SB203580's pyridine and 4-fluorophenyl rings. H-bond and pi-cation interactions were formed between the sidechain of VAL38 and imidazole and the sidechain of VAL38 and fluorophenyl ring of the Ctrl inhibitor, respectively. Moreover, the backbones of the LYS53 and MET109 formed conventional H-bonds with SB203580 imidazole N atom and pyridine, respectively, while HIE107 and LEU108 formed non-classical H-bonds (C-H) with the pyridine ring.

NDPPC docked at the p38 α MAP kinase ATP-binding site (**Figure 4A-C**) showed similar interaction types between NDPPC and interacting residues and per-residues energy contributions, respectively. For the NDPPC-bound ATP site, VAL38 (-2.327 kcal/mol), ALA51 (~ -1.0 kcal/mol), LYS53 (-2.063 kcal/mol), and LEU104 (-1.336 kcal/mol) contributed the most energy. TYR35 and VAL38 contributed the least energy and the highest energy, respectively, to the binding of NDPPC to the ATP-binding site. All the interactions between the NDPPC and p38 α MAP kinase ATP binding site residues were strong hydrophobic but largely van der Waals forces. The backbone of the TYR35 formed strong pi-pi stacked with the pyridine ring of NDPPC and formed pi-alkyl with the methyl group on the ring. In addition, VAL51, ALA51, and LYS53 interacted with the carbothioamide ring of the NDPPC to produce alkyl hydrophobic interactions. Contrary to the interaction of the NDPPC at the ATP-binding site, NCT503 interacted with proximal active site residues, including GLN128, ASP125, HIE126, and CIS162. Except for the HIE126, which contributed about -8.0 kcal/mol energy to the binding, the ASP125 (-0.1 kcal/mol), GLN128 (-0.1 kcal/mol), and CIS162 (-0.6 kcal/mol) contributed low binding energy to NCT503 binding. As a result, the total binding free energy (ΔG value) of the NCT503-p38 α MAP kinase ATP-binding complex is the lowest among the complexes (**Figure 5A-C**).

2.3. Thermodynamics analysis of the interaction with the p38 α MAPK

Thermodynamic calculations provide quantitative mechanistic insights into the binding profile of p38 α MAP kinase inhibitors. The binding free energies of the SB203580, NDPPC, and NCT503 binding at the p38 α MAP kinase (N-terminal domain) site were calculated using the Molecular mechanics with the generalized Born/Poisson-Boltzmann and surface area solvation (MM/PBSA) method provided in the AMBER14 package (Devnarain & Soliman, 2018; Genheden & Ryde, 2015). Our MM/PBSA calculations showed that the compounds exhibited considerably favorable negative energies, indicating strong and high-affinity binding (**Table 1**). We estimated the comparative binding free energy values of the SB203580, NDPPC, and NCT503 to p38 α MAP kinase using the trajectories obtained from the MD simulation. Interestingly, NDPPC had the highest possible minimum energy ($\Delta G = -32.01$ kcal/mol) upon binding to the ATP-binding site compared to the standard inhibitor and NCT503 binding to the ATP binding site. The favourable binding free energy may be associated with the high van der Waal and low electrostatic interactions, corroborating the findings in **Figure 4**. The NCT503 docked at the ATP binding site showed the lowest possible minimum energy ($\Delta G = -14.89$ kcal/mol). Therefore, the highest

favourable minimum energy of the NDPPC-bound at the ATP binding site could correlate with a high affinity and better inhibitory activity (in vitro) of NDPPC compared to the SB203580 and NCT503. The MMGBSA findings revealed that the binding free energy of the NDPPC-bound ATP site of p38 α MAP kinase after MD simulation is more reliable than the molecular docking calculation.

2.4. NDPPC inhibits p38 α MAP kinase activity and augments the 4F-induced cell cycle in CMs

To validate the *In Silico* findings, first, we investigated the inhibitory effect of NDPPC on p38 α MAP kinase activity using a p38 α MAP kinase *in vitro* activity assay. NDPPC and SB203080 directly inhibited p38 α MAPK kinase activity in a dose-dependent manner, while NCT503 did not affect p38 α MAP kinase activity (**Figure 6**). To investigate whether the inhibitory effect of NDPPC on p38 α MAP kinase is the key limiting step in augmenting the 4F-induced cell cycle induction, we overexpressed human p38 α MAP kinase or knocked it down in 60-day-old mature hiPS-CMs for 48 h using lentiviral constructs. The overexpression and the knockdown were confirmed using qRT-PCR (**Figure 7A-B**). As expected, p38 α MAP kinase overexpression inhibited the cell cycle induction in response to 4F, as indicated by a significant decrease in PHH3 and EDU staining in 4F-infected cells (**Figure 7C**). However, the addition of 1 μ M NDPPC reverses the inhibitory effect of p38 α MAP kinase overexpression on cell cycle induction (**Figure 7D**). Furthermore, the knockdown of p38 α MAP kinase in hiPS-CMs augments the number of cardiomyocytes that enter the cell cycle in response to 4F, and the addition of NDPPC did not show any further increase in the cell cycle markers (PHH3 and EDU) (**Figure 7E**). These data indicate that p38 α MAP kinase is the target gene for the NDPPC effect on the 4F-induced cardiomyocyte proliferation. NDPPC inhibits the p38 α MAP kinase activity and increases the response to the 4F-induced cell cycle.

3. Discussion and Conclusions

We and others previously showed that cardiomyocyte cell cycle induction after MI leads to a significant functional improvement in the heart (Abouleisa et al., 2022; Mohamed et al., 2018; Salama et al., 2022; Salama et al., 2021; Shapiro et al., 2014). In addition, our previous studies showed that 4F is an effective tool for inducing cell cycle and complete cytokinesis, which results in improved cardiac function after MI (Abouleisa et al., 2022; Mohamed et al., 2018). However, only 20% of 4F-expressing cardiomyocytes enter the cell cycle and proliferate (Mohamed, Abouleisa, & Hill, 2022; Mohamed et al., 2018). Additional factors that would augment the number of cardiomyocytes to enter the cell cycle and proliferate are required to further improve cardiac function after MI. In this study, we demonstrated that the small molecule, NDPPC, could augment the number of cardiomyocytes that enter the cell cycle in response to 4F.

NDPPC is a small molecule developed to act as inactive control to another small molecule (NCT503). NCT503 is a potent inhibitor of the PHGDH enzyme that plays a critical role in regulating the serine

biosynthetic metabolic pathway (Pacold et al., 2016). Interestingly, our results showed that NDPPC enhances the effect of the 4F-induced cell cycle, but it did not induce cell cycle entry at the baseline. Therefore, NDPPC was screened against the known Homo sapiens targets that play a role in CM proliferation. *In Silico* docking analysis, predicted p38 α MAP kinase as a possible target for NDPPC. Following comprehensive *In Silico* interaction analyses, we demonstrated that the binding free energy (BFE) of the NDPPC-ATP-binding site p38 α MAP kinase (-32.01 kcal/mol) is comparable to the known p38 α MAP kinase inhibitor (SB203580) but significantly higher than the NCT503 at the ATP-binding site p38 α MAP kinase. The mechanism of inhibiting the activity of the p38 α MAP kinase at the ATP binding site occurs via highly energetic hydrophobic interactions (alkyl, pi-alkyl, and pi-pi forces) between the residues TYR35, VAL38, ALA51, LYS53, and LEU104 and the NDPPC functional groups (carbothioamide and pyridine ring).

Moreover, the NDPPC-bound p38 α MAP kinase ATP-binding site (RMSD/1.87, RMSF/1.08) was the most stable and less erratically fluctuated among the systems, including unbound and bound p38 α MAP kinase (**see Supplementary Results and Supplementary figures 2-4**). Therefore, the ATP binding site gave the highest binding free energy with NDPPC. Thus, NDPPC is a likely inhibitor for p38 α MAP kinase through interacting with the ATP binding site of the enzyme.

p38 α MAP kinase has been shown to induce cell cycle exit and differentiation of many cell types, including cardiomyocytes (Ambrosino & Nebreda, 2001; Bulavin, Amundson, & Fornace, 2002; Engel et al., 2005; Eriksson & Leppa, 2002; Nebreda & Ferby, 2000; Shi & Gaestel, 2002; Wu et al., 2000). There are four different p38 MAP kinase isoforms; p38 α MAP kinase is the main isoform expressed in the heart (Liang & Molkentin, 2003; Liao et al., 2001; X. S. Wang et al., 1997). A recent study has shown that p38 α MAP kinase overexpression prevents fetal cardiomyocyte proliferation *in vitro* and *in vivo* (Engel et al., 2005). Whereas targeted disruption of p38 α MAP kinase increases neonatal and adult cardiomyocyte mitosis (Engel et al., 2005). It is also shown that activated p38 α MAP kinase phosphorylates downstream signaling molecules important for the cardiomyocyte differentiation (Liang & Molkentin, 2003). These studies indicated that p38 α MAP kinase is mainly involved in the cardiomyocyte cell cycle's mitosis stage. The *in silico* prediction data was confirmed by our findings that NDPPC but not NCT503 directly inhibits p38 α MAP kinase activity in a dose-dependent manner. Furthermore, we also confirmed the effect of NDPPC on the p38 α MAP kinase pathway by correcting the phenotype of p38 α MAP kinase overexpression on 4F-induced proliferation in cardiomyocytes. Our previous study showed that 4F induces cell cycle reprogramming through increasing cell cycle gene expression and reducing cell cycle inhibitor expression, including p38 MAP kinase (Abouleisa et al., 2022). Therefore, further inhibition of p38 α MAP kinase using NDPPC augmented the 4F cell cycle response in cardiomyocytes.

This study highlighted an off-target effect of the NDPPC, which has been used as a negative and inactive control of NCT503 (Pacold et al., 2016). NDPPC did not inhibit the PHGDH enzyme, and in turn, NDPPC did not inhibit the serine biosynthetic metabolic pathway (Pacold et al., 2016). Our study showed an off-

target effect of the NDPPC, which augments the 4F-induced cell cycle through inhibition of p38 α MAP kinase. Off-target effects of small molecules have been identified before in several studies, which might result in toxicity or other side effects (Al Ibrahim et al., 2022; Rudmann, 2013; Salmasi et al., 2016).

In summary, the results of this study suggest that NDPPC is a novel small molecule inhibitor to the p38 α MAPK activity. Furthermore, NDPPC primes more cardiomyocytes to enter the cell cycle in response to the 4F. NDPPC could be a promising small molecule for adjunct treatment with the cell cycle activators to regenerate the heart and treat ischemia-induced heart failure.

4. Materials and Methods

4.1. Cell Culture: The methods used in this study were performed in accordance with biosafety guidelines approved by the University of Louisville. Human iPSC cardiomyocytes (hiPSC-CMs) were purchased from Fujifilm Cellular Dynamics (cat. R1106). Cells were seeded in Plating Medium (Fujifilm Cellular Dynamics M1001) into plates coated with 0.02% gelatin (Sigma Aldrich 9000-70-8) and 0.01% fibronectin (Sigma Aldrich cat. F1141). The hiPSC-CMs were maintained for a minimum of 3-4 weeks prior to experimentation in a maintenance medium (Fujifilm Cellular Dynamics cat. M1003) supplemented with 1% penicillin/streptomycin (ThermoFisher 15070063).

4.2. Adenoviral Transduction: hiPSC-CMs were transduced with adenovirus at the following MOI: LacZ and 4F (Cdk1, Ccnb, Cdk4, Ccnd) 10 MOI each; Adenoviruses were removed after 24 h and replaced with maintenance medium for another 24 h.

4.3. Drug intervention: NCT503 (Millipore Sigma, SML 1659), NDPPC (Millipore Sigma, SML1671), and SB203580 (ab120162) were diluted to 10 mM in DMSO and then diluted to the required concentration in PBS.

4.4. Immunocytochemistry and EdU incorporation: hiPS-CMs were fixed in 4% formaldehyde for 20 min (Thermos Scientific Cat#28908). Fixed cells were washed three times with PBS. Next, the fixed cells were permeabilized with 0.1% Triton X-100 for 15 min (Millipore Cat# 55163804) and then blocked with 3% bovine serum albumin (BSA) in PBS for 60 min at room temperature (VWR Cat# 0332). The cells were then probed with Mouse Monoclonal Cardiac Troponin T Antibody (Thermos Fisher, MA5-12960) and rabbit monoclonal Anti-Histone H3 (phospho S10) antibody - ChIP Grade (Abcam; ab5176) primary antibody (1:200 in 1% BSA) for 1.5 hours. They were then washed three times with PBS. Then labeled with Goat anti-Mouse IgG (H+L), FITC (Thermofisher, A16079), and Texas Red Goat anti-Rabbit IgG (H+L) (Thermos fisher, T-6391) secondary fluorescent antibody respectively (1:200 in 1% BSA). Next, cells were washed three times with PBS and stained with DAPI 1 μ g/ml (Biotium Cat# 40043) to stain the nucleus blue. For EDU detection, the cells were also treated with 5 μ M 5-ethyl-2-deoxyuridine (EDU) for the course of the experiment, which will incorporate into the newly synthesized DNA. After fixation, permeabilization, and blocking of the cells, the EDU incorporation was visualized using the Click it EDU-

Alexa-Fluor⁶⁴⁷ imaging kit (ThermoFisher, C10340). Imaging was conducted for the whole well using the high-content imaging instrument, Cytation 1. The percentage of colocalization of PHH3, EDU, and Troponin-T was quantified using Gen 5.05 software.

4.5. qRT-PCR: hiPS-CMs were mixed with QIAzol lysis reagent (Qiagen Cat# 79306), then RNA was extracted following the miRNeasy micro kit protocol (Qiagen Cat# 217084). The concentration of the RNA was calculated using the Cytation 1 reader. 0.2ug of each RNA sample was used for reverse transcription using a mixture of oligo(dT) and random hexamer primers (SuperScript IV VILO Master Mix, ThermoFisher Scientific Cat # 11756050). Real-time PCR analysis was conducted with Taqman fast advanced master mix (ThermoFisher 4444557) and primers specific to human p38 MAPK genes (Applied Biosystems# 01051152), and the expression was normalized to human GAPDH expression (Applied Biosystems# 2786624) using the Quant studio5 real-time PCR detection system (Applied Biosystems).

4.6. p38 α MAP kinase activity assay: p38 α MAP kinase enzyme assay kit (Promega V2701) was used to test the effect of NDPPC, NCT503, SB203580 on the p38 α MAP kinase activity following the manufacture protocol. In brief, 6.3ng of p38 α MAP kinase protein was added to 50 μ M ATP and substrate mixture. This mixture is treated with a vehicle or different concentration of the assigned drug. The mixture was kept at RT for 1 h. Then, the Kinase Glo Max luminescent kinase assay kit (Promega V6071) was used to detect the amount of ATP present. The P38 α activity was calculated based on the amount of ATP detected.

4.7. System preparation and molecular docking study: The x-ray crystal of human unphosphorylated, low-activity MAP kinase p38 protein was obtained from the RCSB Protein Data bank with ID 1A9U (Wang et al., 1998). The system was prepared using UCSF Chimera (A. T. Adewumi, Elrashedy, Soremekun, Ajadi, & Soliman, 2022; Pettersen et al., 2004; Yang et al., 2012) to remove co-crystallized molecules, including the control inhibitor SB203580 bound at the ATP-binding site of p38 MAP kinase. NDPPC and NCT503 were drawn in the GaussView-6.0, cleaned, and symmetrized. Further ligand optimization was performed using Avogadro-1.95 (Hanwell et al., 2012). Similarly, the ligands were using the Chimera tool and saved in mol2 format (Yang et al., 2012). The add-on GAFF in Avogadro-1.2.0n⁴ minimized the molecules (<http://avogadro.cc/>). The compounds were assessed in the Molegro Molecular Viewer-2.5 (<http://molexus.io/molegro-molecular-viewer>) for bond angles and hybridization state correctness. Flexible docking calculation was carried out using Autodock-1.5.6 (Fu, Zhao, & Chen, 2018). The p38 α MAP kinase receptor and ligands were further prepared in the Autodock tool by adding essential non-polar hydrogen atoms, charges, and solvation parameters saved in pdbqt files (Morris et al., 2009). The SB203580, NDPPC, and NCT503 were docked separately at the ATP-binding site. Each active site's grid box was defined using the Autodock graphical interface (Morris et al., 2009). The grid box was centered around the ATP-binding site and defined the center as X = 2.292, Y = 15.574, and Z = 29.532 with dimensions X = 72, Y = 80, and Y = 56 (Trott & Olson, 2010) The ATP-binding site includes residues

TYR35, VAL38, ALA51, VAL52, LYS53, GLU71, LEU75, ILE84, GLY85, LEU86, LEU104, VAL105, THR106, HIS107, LEU108, MET109, ASP168, and ARG173. Docking calculations were performed using the Lamarckian Genetic Algorithm (LGA) with ten iterative runs (Fu et al., 2018).

4.8. Molecular dynamics simulations and thermodynamics calculation: This study used apo and five ligand-bound p38 MAP systems for molecular dynamics (MD) simulations with the graphic processor unit (GPU) version of AMBER18, integrated CUDA engine, and LEAP modules (Case et al., 2005) The study objective investigates the inhibitory mechanisms of the two proposed inhibitors bound separately at the ATP-binding site. The simulation study was carried out using modified methods in our previous works. The studied systems were parameterized using the AMBER FF14SB Force Field. The systems' topologies were created with the LEAP module that introduced hydrogen atoms and neutralized the systems. The pdb4amber script was performed to protonate the histidine residues at a constant pH before running the LEAP module, which modifies the p38 α MAP kinase for compatibility with the leap. Moreover, all atoms explicit solvation method was used in which the process occurred in a 12 Å orthorhombic TIP3P box containing water molecules (Mark & Nilsson, 2001). The systems were partially minimized with 500 kcal/mol restraint potential for 2500 steps and fully minimized for 5000 steps. The systems were heated up gradually from 0 to 300 K. The unliganded and bound systems were equilibrated for 1 nanosecond at 300 K while using the Berendsen barostat to keep the pressure at 1 bar (Adeniyi T. Adewumi, Soremekun, Ajadi, & Soliman, 2020; Berendsen, Postma, van Gunsteren, DiNola, & Haak, 1984). The production MD simulations step was carried out for 200 nanoseconds. The integrated CPPTRAJ and PTRJ modules implemented in AMBER18 were used to generate the output coordinates and printed trajectories (Roe & Cheatham, 2013). The visual analysis of structures was performed using combined graphical interfaces of the UCSF Chimera (Yang et al., 2012), Molegro Molecular Viewer (Devnarain & Soliman, 2018), and BIOVIA Discovery Studio (A. T. Adewumi et al., 2022). Lastly, the data were processed with MicroCal Origin-6.0 data software (Seifert, 2014). Furthermore, the binding free energies of the NDPPC and NCT503 binding at the p38 α MAP kinase ATP (N-terminal domain) site were calculated using the Molecular mechanics with the generalized Born/Poisson-Boltzmann and surface area solvation (MMGB(PB)SA) method provided in the AMBER14 package (Devnarain & Soliman, 2018; Genheden & Ryde, 2015). This method has been widely applied in our previously published articles (Oluyemi et al., 2022). We used 200 snapshots from the 40 000 frames of the MD simulation trajectories obtained at every 200 ps (Daina, Michielin, & Zoete, 2014; Ndlovu et al., 2019). The MMPB(GB)SA calculation is mathematically given as follows:

$$\Delta G_{\text{MMPB(GB)SA}} = \Delta G_{\text{ele}} + \Delta G_{\text{vdW}} + \Delta G_{\text{int}} + \Delta G_{\text{nonpol}} + \Delta G_{\text{pol}} \dots\dots\dots(\text{i})$$

$$\Delta G_{\text{bind}} = E_{\text{gas}} + G_{\text{sol}} - TS \dots\dots\dots (\text{ii})$$

$$E_{\text{gas}} = E_{\text{int}} + E_{\text{vdw}} + E_{\text{ele}} \dots\dots\dots (\text{iii})$$

$$G_{\text{sol}} = G_{\text{GB}} + G_{\text{SA}} \dots\dots\dots (\text{iv})$$

References

- Abouleisa, R. R. E., McNally, L., Salama, A. B. M., Hammad, S. K., Ou, Q., Wells, C., ... Hill, B. G. (2021). Cell cycle induction in human cardiomyocytes is dependent on biosynthetic pathway activation. *Redox Biol*, *46*, 102094. doi:10.1016/j.redox.2021.102094
- Abouleisa, R. R. E., Salama, A. B. M., Ou, Q., Tang, X. L., Solanki, M., Guo, Y., ... Mohamed, T. M. A. (2022). Transient Cell Cycle Induction in Cardiomyocytes to Treat Subacute Ischemic Heart Failure. *Circulation*, *145*(17), 1339-1355. doi:10.1161/CIRCULATIONAHA.121.057641
- Adewumi, A. T., Elrashedy, A., Soremekun, O. S., Ajadi, M. B., & Soliman, M. E. S. (2022). Weak spots inhibition in the Mycobacterium tuberculosis antigen 85C target for antitubercular drug design through selective irreversible covalent inhibitor-SER124. *J Biomol Struct Dyn*, *40*(7), 2934-2954. doi:10.1080/07391102.2020.1844061
- Adewumi, A. T., Soremekun, O. S., Ajadi, M. B., & Soliman, M. E. S. (2020). Thompson loop: opportunities for antitubercular drug design by targeting the weak spot in demethylmenaquinone methyltransferase protein. *RSC Advances*, *10*(39), 23466-23483. doi:10.1039/D0RA03206A
- Al Ibrahim, A. H., Ghallab, K. Q., Alhumaid, F. I., Almahfoudh, H. H., Almadan, A. J., Al Eid, M. A., ... Aljamea, J. H. (2022). A Systematic Review of Sildenafil Mortality Through the Years. *Cureus*, *14*(12), e32179. doi:10.7759/cureus.32179
- Ambrosino, C., & Nebreda, A. R. (2001). Cell cycle regulation by p38 MAP kinases. *Biol Cell*, *93*(1-2), 47-51. doi:10.1016/s0248-4900(01)01124-8
- Berendsen, H. J. C., Postma, J. P. M., van Gunsteren, W. F., DiNola, A., & Haak, J. R. (1984). Molecular dynamics with coupling to an external bath. *Journal of Chemical Physics*, *81*, 3684-3690. doi:10.1063/1.448118
- Birkenkamp, K. U., Tuyt, L. M., Lummen, C., Wierenga, A. T., Kruijer, W., & Vellenga, E. (2000). The p38 MAP kinase inhibitor SB203580 enhances nuclear factor-kappa B transcriptional activity by a non-specific effect upon the ERK pathway. *Br J Pharmacol*, *131*(1), 99-107. doi:10.1038/sj.bjp.0703534
- Bulavin, D. V., Amundson, S. A., & Fornace, A. J. (2002). p38 and Chk1 kinases: different conductors for the G(2)/M checkpoint symphony. *Curr Opin Genet Dev*, *12*(1), 92-97. doi:10.1016/s0959-437x(01)00270-2
- Case, D. A., Cheatham, T. E., 3rd, Darden, T., Gohlke, H., Luo, R., Merz, K. M., Jr., ... Woods, R. J. (2005). The Amber biomolecular simulation programs. *J Comput Chem*, *26*(16), 1668-1688. doi:10.1002/jcc.20290
- Daina, A., Michielin, O., & Zoete, V. (2014). iLOGP: A Simple, Robust, and Efficient Description of n-Octanol/Water Partition Coefficient for Drug Design Using the GB/SA Approach. *Journal of Chemical Information and Modeling*, *54*(12), 3284-3301. doi:10.1021/ci500467k
- Devnarain, N., & Soliman, M. E. S. (2018). A panoptic uncovering of the dynamical evolution of the Zika Virus NS5 methyltransferase binding site loops-zeroing in on the molecular landscape. *Chem Biol Drug Des*, *92*(5), 1838-1850. doi:10.1111/cbdd.13353
- Engel, F. B., Schebesta, M., Duong, M. T., Lu, G., Ren, S., Madwed, J. B., ... Keating, M. T. (2005). p38 MAP kinase inhibition enables proliferation of adult mammalian cardiomyocytes. *Genes Dev*, *19*(10), 1175-1187. doi:10.1101/gad.1306705
- Eriksson, M., & Leppa, S. (2002). Mitogen-activated protein kinases and activator protein 1 are required for proliferation and cardiomyocyte differentiation of P19 embryonal carcinoma cells. *J Biol Chem*, *277*(18), 15992-16001. doi:10.1074/jbc.M107340200
- Fu, Y., Zhao, J., & Chen, Z. (2018). Insights into the Molecular Mechanisms of Protein-Ligand Interactions by Molecular Docking and Molecular Dynamics Simulation: A Case of Oligopeptide Binding Protein. *Comput Math Methods Med*, *2018*, 3502514. doi:10.1155/2018/3502514
- Genheden, S., & Ryde, U. (2015). The MM/PBSA and MM/GBSA methods to estimate ligand-binding affinities. *Expert Opin Drug Discov*, *10*(5), 449-461. doi:10.1517/17460441.2015.1032936
- Haar, E. T., Prabakhar, P., Liu, X., & Lepre, C. (2007). Crystal structure of the p38 alpha-MAPKAP kinase 2 heterodimer. *J Biol Chem*, *282*(13), 9733-9739. doi:10.1074/jbc.M611165200

- Hanwell, M. D., Curtis, D. E., Lonie, D. C., Vandermeersch, T., Zurek, E., & Hutchison, G. R. (2012). Avogadro: an advanced semantic chemical editor, visualization, and analysis platform. *J Cheminform*, 4(1), 17. doi:10.1186/1758-2946-4-17
- Hollingsworth, S. A., & Dror, R. O. (2018). Molecular Dynamics Simulation for All. *Neuron*, 99(6), 1129-1143. doi:10.1016/j.neuron.2018.08.011
- Hydbring, P., Malumbres, M., & Sicinski, P. (2016). Non-canonical functions of cell cycle cyclins and cyclin-dependent kinases. *Nat Rev Mol Cell Biol*, 17(5), 280-292. doi:10.1038/nrm.2016.27
- Ioacara, S., Popescu, A. C., Tenenbaum, J., Dimulescu, D. R., Popescu, M. R., Sirbu, A., & Fica, S. (2019). Acute Myocardial Infarction Mortality Rates and Trends in Romania between 1994 and 2017. *Int J Environ Res Public Health*, 17(1)doi:10.3390/ijerph17010285
- Johnson, J., Mohsin, S., & Houser, S. R. (2021). Cardiomyocyte Proliferation as a Source of New Myocyte Development in the Adult Heart. *Int J Mol Sci*, 22(15)doi:10.3390/ijms22157764
- Liang, Q., & Molkentin, J. D. (2003). Redefining the roles of p38 and JNK signaling in cardiac hypertrophy: dichotomy between cultured myocytes and animal models. *J Mol Cell Cardiol*, 35(12), 1385-1394. doi:10.1016/j.yjmcc.2003.10.001
- Liao, P., Georgakopoulos, D., Kovacs, A., Zheng, M., Lerner, D., Pu, H., ... Wang, Y. (2001). The in vivo role of p38 MAP kinases in cardiac remodeling and restrictive cardiomyopathy. *Proc Natl Acad Sci U S A*, 98(21), 12283-12288. doi:10.1073/pnas.211086598
- Malumbres, M., & Barbacid, M. (2009). Cell cycle, CDKs and cancer: a changing paradigm. *Nat Rev Cancer*, 9(3), 153-166. doi:10.1038/nrc2602
- Mark, P., & Nilsson, L. (2001). Structure and Dynamics of the TIP3P, SPC, and SPC/E Water Models at 298 K. *The Journal of Physical Chemistry A*, 105(43), 9954-9960. doi:10.1021/jp003020w
- Mohamed, T. M. A., Abouleisa, R., & Hill, B. G. (2022). Metabolic Determinants of Cardiomyocyte Proliferation. *Stem Cells*, 40(5), 458-467. doi:10.1093/stmcls/sxac016
- Mohamed, T. M. A., Ang, Y. S., Radzinsky, E., Zhou, P., Huang, Y., Elfenbein, A., ... Srivastava, D. (2018). Regulation of Cell Cycle to Stimulate Adult Cardiomyocyte Proliferation and Cardiac Regeneration. *Cell*, 173(1), 104-116 e112. doi:10.1016/j.cell.2018.02.014
- Morris, G. M., Huey, R., Lindstrom, W., Sanner, M. F., Belew, R. K., Goodsell, D. S., & Olson, A. J. (2009). AutoDock4 and AutoDockTools4: Automated docking with selective receptor flexibility. *J Comput Chem*, 30(16), 2785-2791. doi:10.1002/jcc.21256
- Ndlovu, S. T., Ullah, N., Khan, S., Ramharack, P., Soliman, M., de Matas, M., ... Hussain, Z. (2019). Domperidone nanocrystals with boosted oral bioavailability: fabrication, evaluation and molecular insight into the polymer-domperidone nanocrystal interaction. *Drug Deliv Transl Res*, 9(1), 284-297. doi:10.1007/s13346-018-00596-w
- Nebreda, A. R., & Ferby, I. (2000). Regulation of the meiotic cell cycle in oocytes. *Curr Opin Cell Biol*, 12(6), 666-675. doi:10.1016/s0955-0674(00)00150-2
- Oluyemi, W. M., Samuel, B. B., Adewumi, A. T., Adekunle, Y. A., Soliman, M. E. S., & Krenn, L. (2022). An Allosteric Inhibitory Potential of Triterpenes from *Combretum racemosum* on the Structural and Functional Dynamics of Plasmodium falciparum Lactate Dehydrogenase Binding Landscape. *Chemistry & Biodiversity*, 19(2), e202100646. doi:<https://doi.org/10.1002/cbdv.202100646>
- Pacold, M. E., Brimacombe, K. R., Chan, S. H., Rohde, J. M., Lewis, C. A., Swier, L. J., ... Sabatini, D. M. (2016). A PHGDH inhibitor reveals coordination of serine synthesis and one-carbon unit fate. *Nat Chem Biol*, 12(6), 452-458. doi:10.1038/nchembio.2070
- Pettersen, E. F., Goddard, T. D., Huang, C. C., Couch, G. S., Greenblatt, D. M., Meng, E. C., & Ferrin, T. E. (2004). UCSF Chimera--a visualization system for exploratory research and analysis. *J Comput Chem*, 25(13), 1605-1612. doi:10.1002/jcc.20084
- Roe, D. R., & Cheatham, T. E., III. (2013). PTRAJ and CPPTRAJ: Software for Processing and Analysis of Molecular Dynamics Trajectory Data. *Journal of Chemical Theory and Computation*, 9(7), 3084-3095. doi:10.1021/ct400341p

- Rudmann, D. G. (2013). On-target and off-target-based toxicologic effects. *Toxicol Pathol*, 41(2), 310-314. doi:10.1177/0192623312464311
- Salama, A. B. M., Abouleisa, R. R. E., Ou, Q., Tang, X. L., Alhariry, N., Hassan, S., ... Mohamed, T. M. A. (2022). Transient gene therapy using cell cycle factors reverses renin-angiotensin-aldosterone system activation in heart failure rat model. *Mol Cell Biochem* doi:10.1007/s11010-022-04590-2
- Salama, A. B. M., Gebreil, A., Mohamed, T. M. A., & Abouleisa, R. R. E. (2021). Induced Cardiomyocyte Proliferation: A Promising Approach to Cure Heart Failure. *Int J Mol Sci*, 22(14) doi:10.3390/ijms22147720
- Salmasi, A., Lee, G. T., Patel, N., Goyal, R., Dinizo, M., Kwon, Y. S., ... Kim, I. Y. (2016). Off-Target Effect of Sildenafil on Postsurgical Erectile Dysfunction: Alternate Pathways and Localized Delivery System. *J Sex Med*, 13(12), 1834-1843. doi:10.1016/j.jsxm.2016.10.003
- Seifert, E. (2014). OriginPro 9.1: Scientific Data Analysis and Graphing Software—Software Review. *Journal of Chemical Information and Modeling*, 54(5), 1552-1552. doi:10.1021/ci500161d
- Shapiro, S. D., Ranjan, A. K., Kawase, Y., Cheng, R. K., Kara, R. J., Bhattacharya, R., ... Chaudhry, H. W. (2014). Cyclin A2 induces cardiac regeneration after myocardial infarction through cytokinesis of adult cardiomyocytes. *Sci Transl Med*, 6(224), 224ra227. doi:10.1126/scitranslmed.3007668
- Shi, Y., & Gaestel, M. (2002). In the cellular garden of forking paths: how p38 MAPKs signal for downstream assistance. *Biol Chem*, 383(10), 1519-1536. doi:10.1515/BC.2002.173
- Trott, O., & Olson, A. J. (2010). AutoDock Vina: improving the speed and accuracy of docking with a new scoring function, efficient optimization, and multithreading. *J Comput Chem*, 31(2), 455-461. doi:10.1002/jcc.21334
- Wang, X. S., Diener, K., Manthey, C. L., Wang, S., Rosenzweig, B., Bray, J., ... Yao, Z. (1997). Molecular cloning and characterization of a novel p38 mitogen-activated protein kinase. *J Biol Chem*, 272(38), 23668-23674. doi:10.1074/jbc.272.38.23668
- Wang, Z., Canagarajah, B. J., Boehm, J. C., Kassisa, S., Cobb, M. H., Young, P. R., ... Goldsmith, E. J. (1998). Structural basis of inhibitor selectivity in MAP kinases. *Structure*, 6(9), 1117-1128. doi:10.1016/s0969-2126(98)00113-0
- Wang, Z., Harkins, P. C., Ulevitch, R. J., Han, J., Cobb, M. H., & Goldsmith, E. J. (1997). The structure of mitogen-activated protein kinase p38 at 2.1-Å resolution. *Proc Natl Acad Sci U S A*, 94(6), 2327-2332. doi:10.1073/pnas.94.6.2327
- Wu, Z., Woodring, P. J., Bhakta, K. S., Tamura, K., Wen, F., Feramisco, J. R., ... Puri, P. L. (2000). p38 and extracellular signal-regulated kinases regulate the myogenic program at multiple steps. *Mol Cell Biol*, 20(11), 3951-3964. doi:10.1128/MCB.20.11.3951-3964.2000
- Yang, Z., Lasker, K., Schneidman-Duhovny, D., Webb, B., Huang, C. C., Pettersen, E. F., ... Ferrin, T. E. (2012). UCSF Chimera, MODELLER, and IMP: an integrated modeling system. *J Struct Biol*, 179(3), 269-278. doi:10.1016/j.jsb.2011.09.006

Table 1. Thermodynamics parameters between the SB203580, NDPPC, and NCT503 at the ATP-binding site residues of p38 α MAP kinase using the MMPBSA method.

Complex	Energy components (kcal mol ⁻¹)						
	ΔE_{vdW}	ΔE_{elec}	ΔG_{gas}	E_{GB}	E_{SA}	ΔG_{solv}	ΔG_{bind}
SB203580-p38 ATP	-35.19 (± 5.44)	-23.35 (± 11.97)	-58.54 (± 16.31)	34.99 (± 9.67)	-4.75 (± 0.68)	30.24 (± 9.12)	-28.30 (± 8.01)
NDPPC-p38 ATP	-37.34 (± 3.46)	0.31 (± 7.74)	-37.03 (± 9.42)	9.52 (± 7.77)	-4.50 (± 0.46)	5.02 (± 7.50)	-32.01 (± 3.97)
NCT503-p38 ATP	-21.00 (± 5.47)	-233.97 (± 35.19)	-254.98 (± 33.32)	243.17 (± 34.39)	-3.09 (± 0.70)	40.90 (± 34.35)	-14.89 (± 4.58)

(ΔE_{elec} (electrostatic), ΔE_{vdw} (van der Waals), ΔG_{bind} (calculated total free binding energy) ΔG_{gas} (gas-phase energy), ΔG_{solv} (solvation free energy), and ATPS (p38 α MAP kinase protein ATP-binding site of p38 α MAP kinase protein).

Figure legend

Figure 1: NDPPC primes more CMs to enter the cell cycle in response to 4F: (A) Representative images of hiPS-CMs transduced with LacZ or 4F adenovirus and treated with Vehicle, 0.1, 0.5, 1, 5 μ M NDPPC and stained against troponin (green), PHH3 (red), EDU (grey), DAPI (blue) (scale bar 100 μ m). (B) Quantification of %PHH3 and (C) %EDU positive nuclei (n=6 independent experiments each in duplicate, *p<0.05, **p<0.01, ***p<0.001 versus vehicle-4F-transduced CMs, ###p<0.001 versus vehicle-LacZ-transduced cardiomyocytes).

Figure 2: Molecular docking studies showing the binding affinity of NDPPC to human p38 α MAP kinase at the ATP binding site: 3D visualization structure of (A) SB203580, a known inhibitor of p38 α MAP kinase, (B) NDPPC, and (C) overlapped docking poses of SB203580 and NDPPC at the ATP binding site of the human p38 α MAP kinase.

Figure 3. Energy contribution and residue interaction plot p38 α MAP kinase-SB203580. (A) 3D structure of p38 α MAP kinase in complex with SB203580 (B) p38 α MAP kinase-SB203580 residual interaction. (C) The energy contribution of p38 α MAP kinase residues interacting with SB203580

Figure 4. Energy contribution and residue interaction plot p38 ATP site- NDPPC. (A) 3D structure of p38 α MAP kinase in complex with NDPPC (B) p38 α MAP kinase ATP site-NDPPC residual interaction. (C) The energy contribution by p38 α MAP kinase residues interacting with NDPPC.

Figure 5. Energy contribution and residue interaction plot p38 α MAP kinase ATP site NCT503. (A) 3D structure of p38 α MAP kinase in complex with NCT503 (B) p38 α MAP kinase ATP site- NCT503 residual interaction. (C) The energy contribution by p38 α MAP kinase residues interacting with NCT503

Figure 6. NDPPC inhibits human p38 α MAP kinase activity in vitro assay. Quantification of human p38 α MAP kinase activity in the presence of (A) SB203580, (B) NDPPC, or (C) NCT503 using a p38 α MAP kinase assay. (n=2 independent experiments each in triplicate **P<0.01, ****<0.0001).

Figure 7. NDPPC inhibits p38 α MAP kinase and retains the 4F-induced cell cycle induction in p38 α MAP kinase overexpressed hiPS-CMs: (A) Fold change analysis of the mRNA expression of human p38 α MAP kinase in hiPS-CMs transduced with control-integrating lentivirus (ctrl-IL) or p38 α MAP kinase integrating lentivirus (p38-IL) and (B) Knockdown of endogenous p38 α MAP kinase in response to ShRNA-p38-IL transduction (n=2 independent experiments each in triplicate *P<0.05, **<0.01). (C) Representative images of hiPS-CMs transduced with 4F, 4F+ShRNA-p38-IL, or 4F+p38-IL and treated with either vehicle or 1 μ M NDPPC, and immunostained for troponin-T (green), DAPI (blue), PHH3 (red),

and EDU (gray) (scale bar=100 μ m). **(D)** Quantification of the percentage of cardiomyocyte-positive nuclei for the cell cycle markers PHH3 and **(E)** EDU (n=4 independent experiments each in duplicate, *p<0.05, **p<0.01, ***p<0.001).

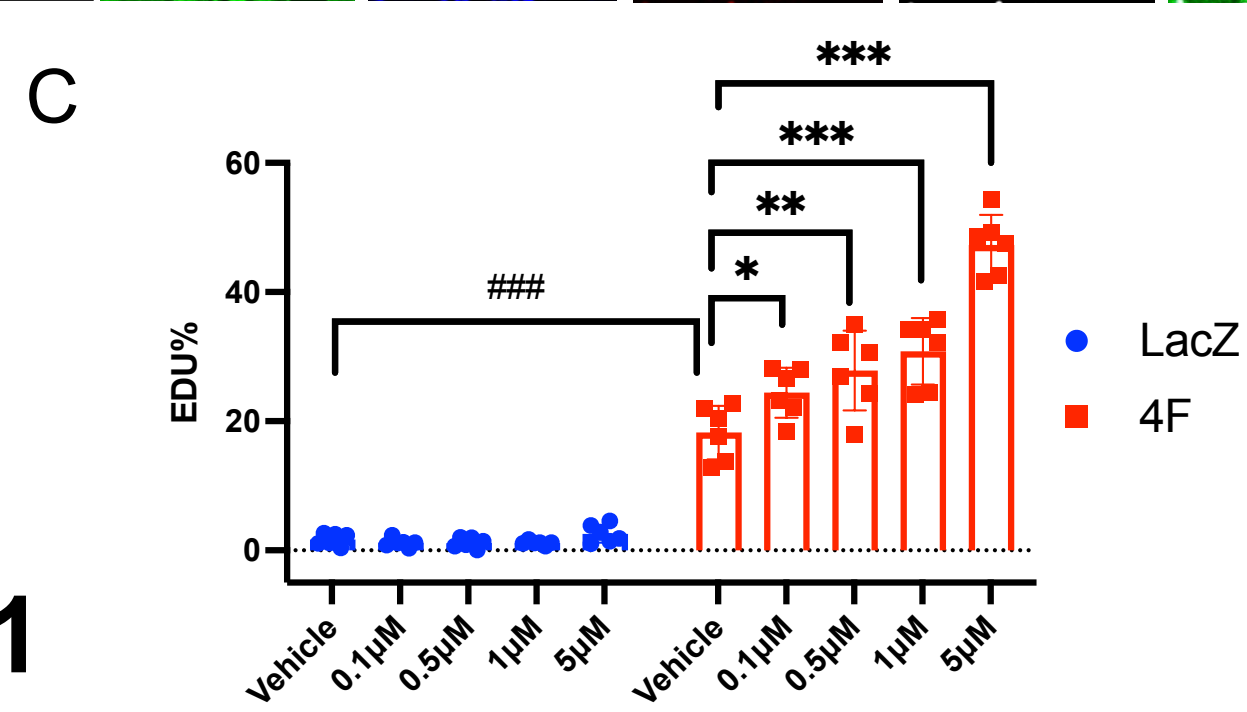
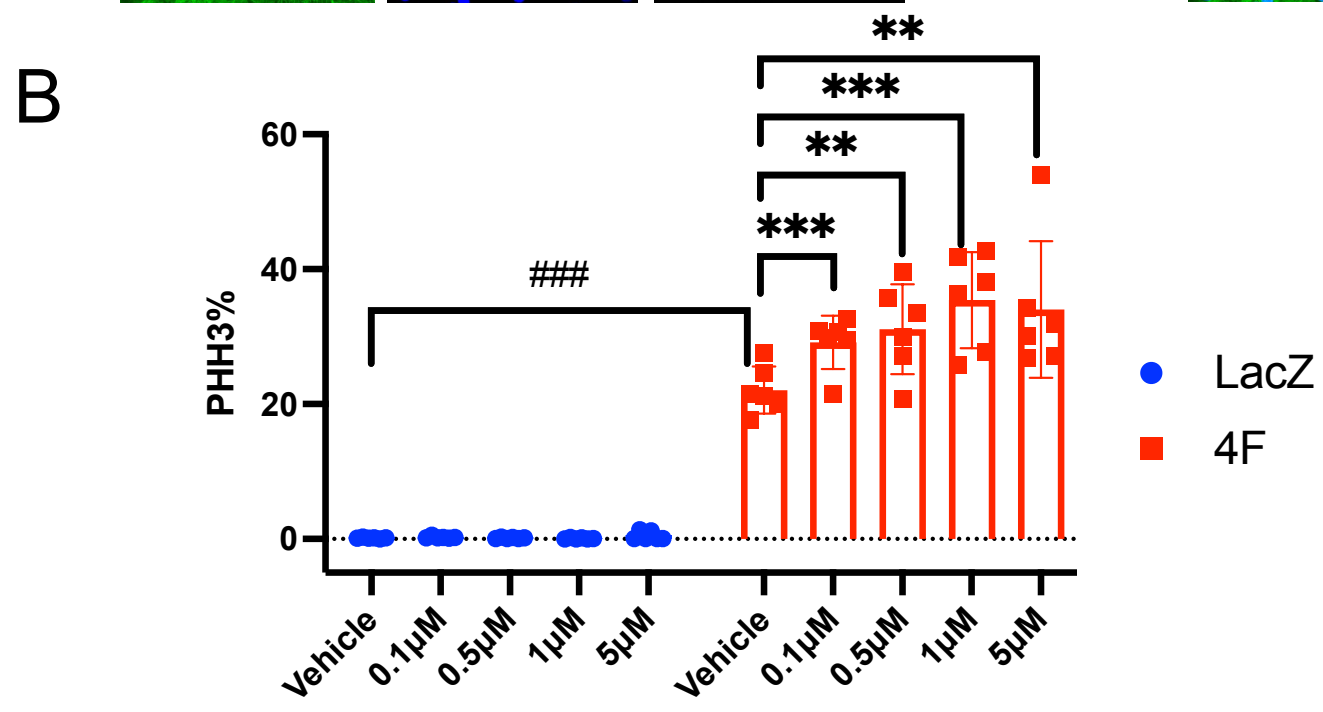
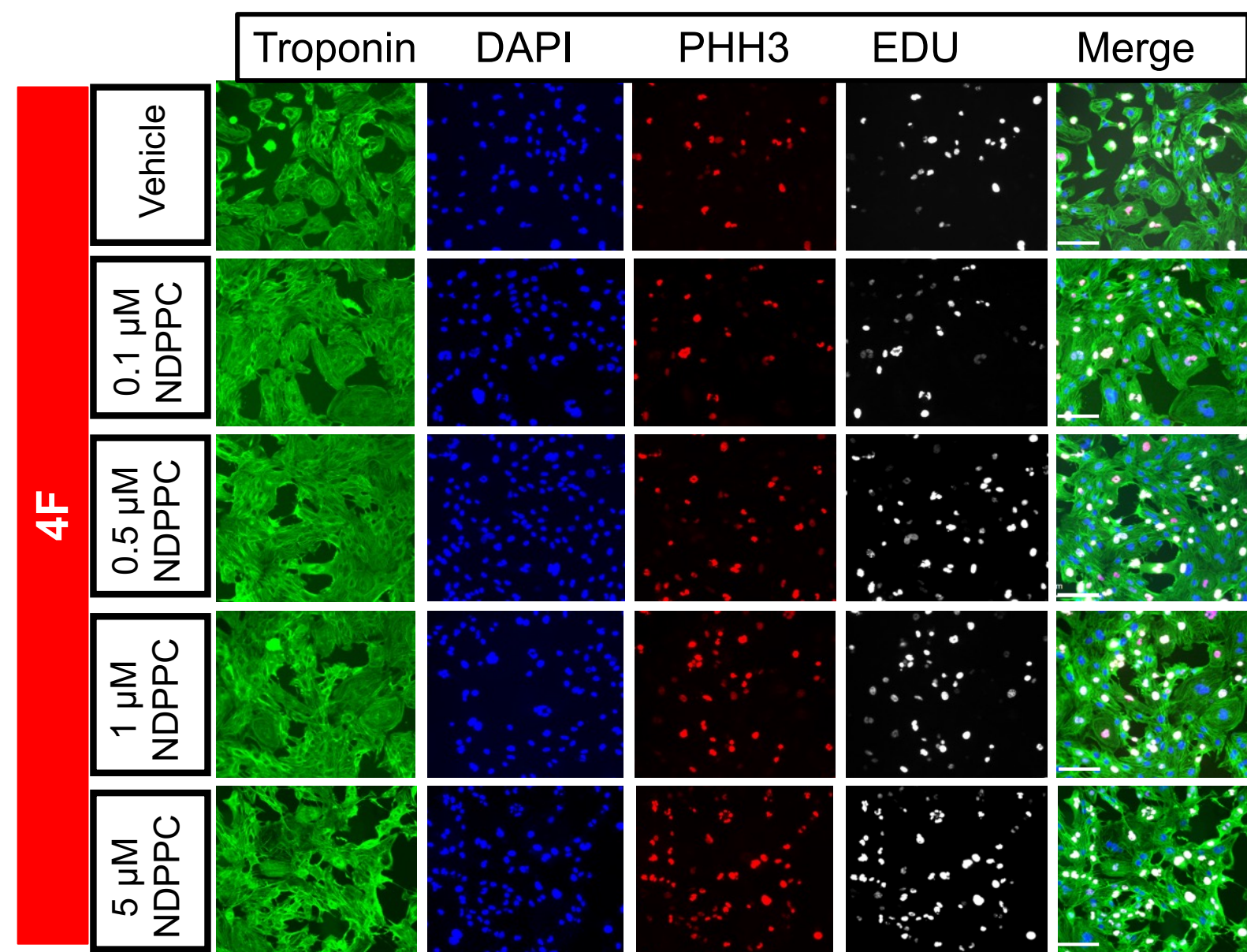
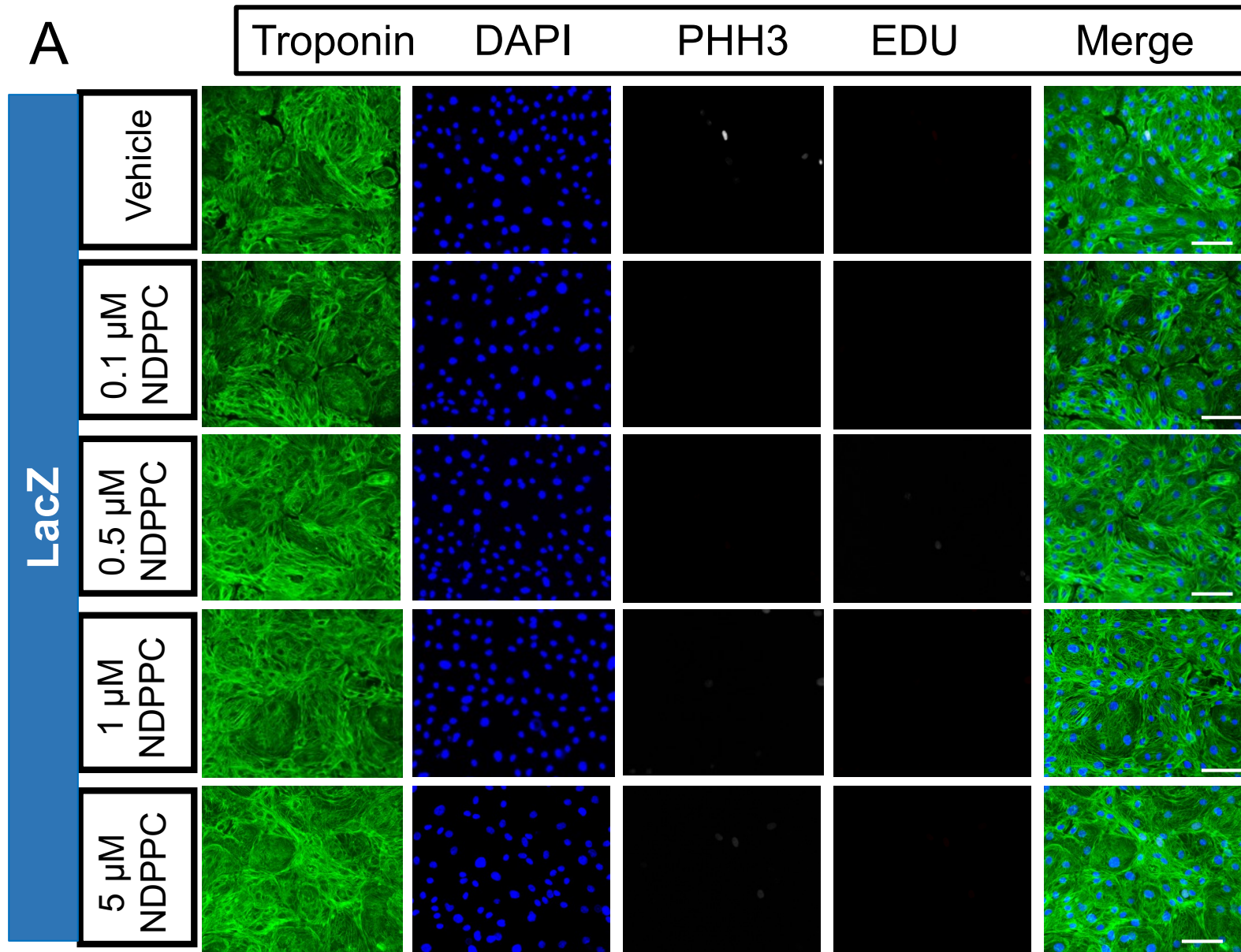
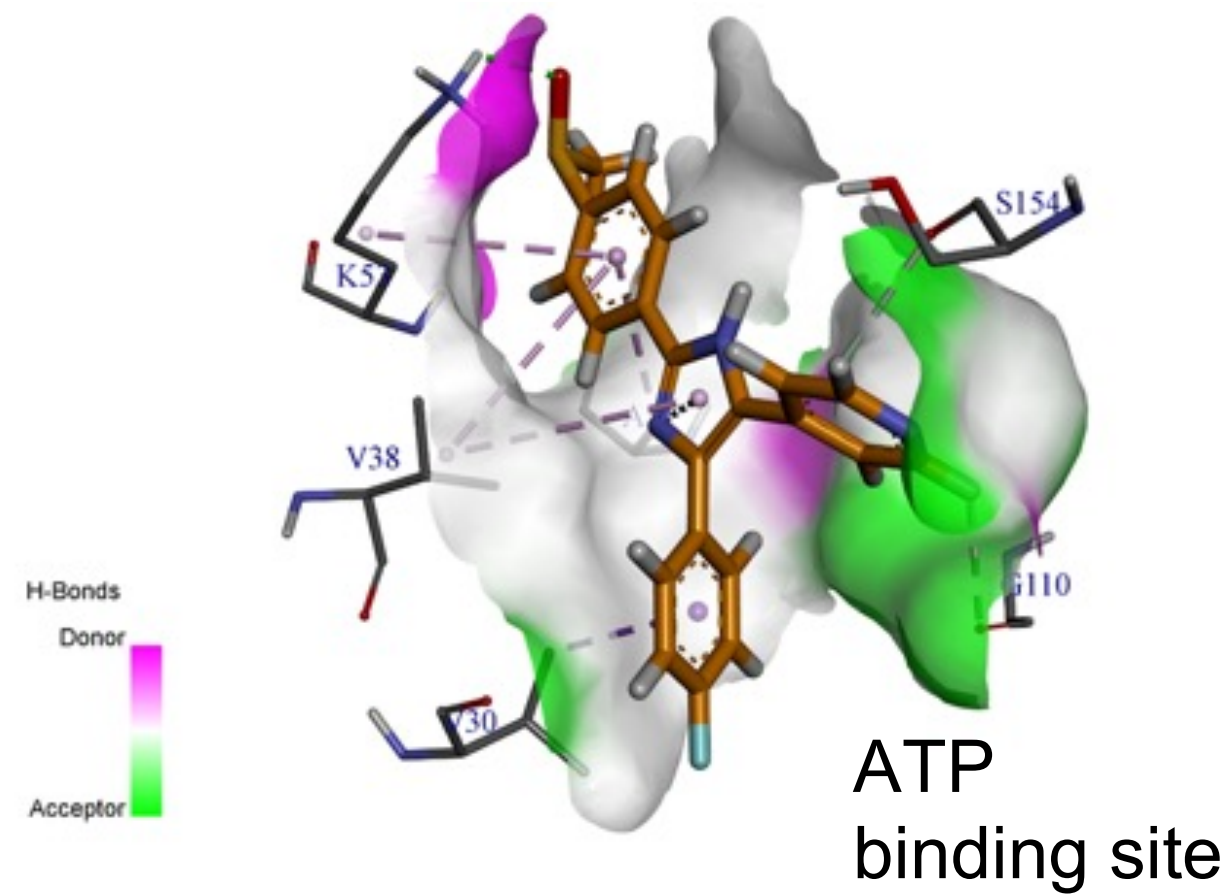


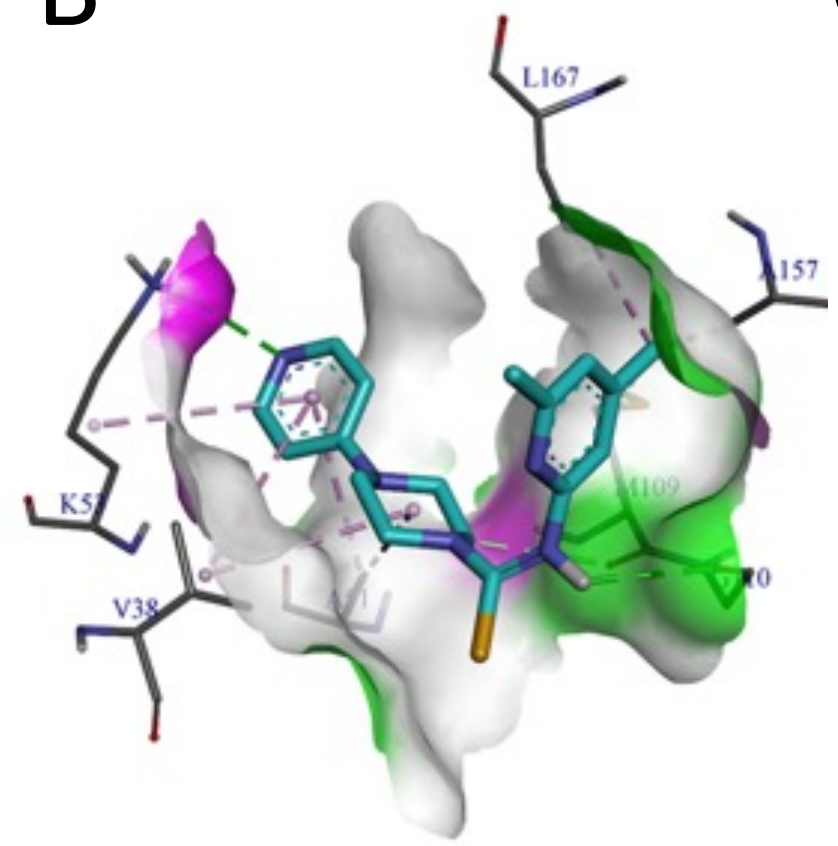
Figure 1

Figure 2

A



B



C

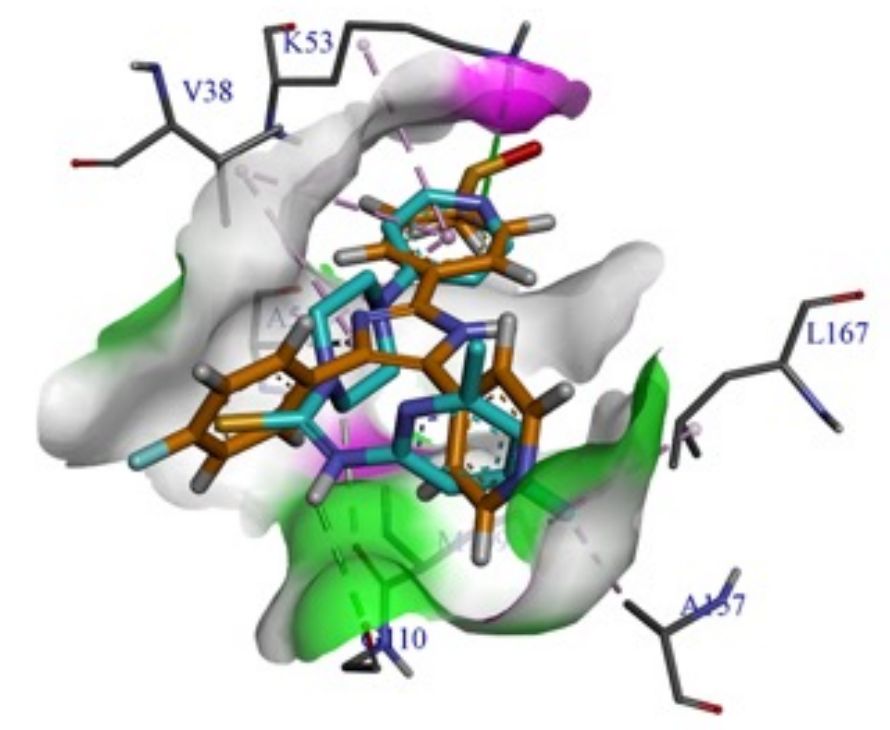


Figure 3

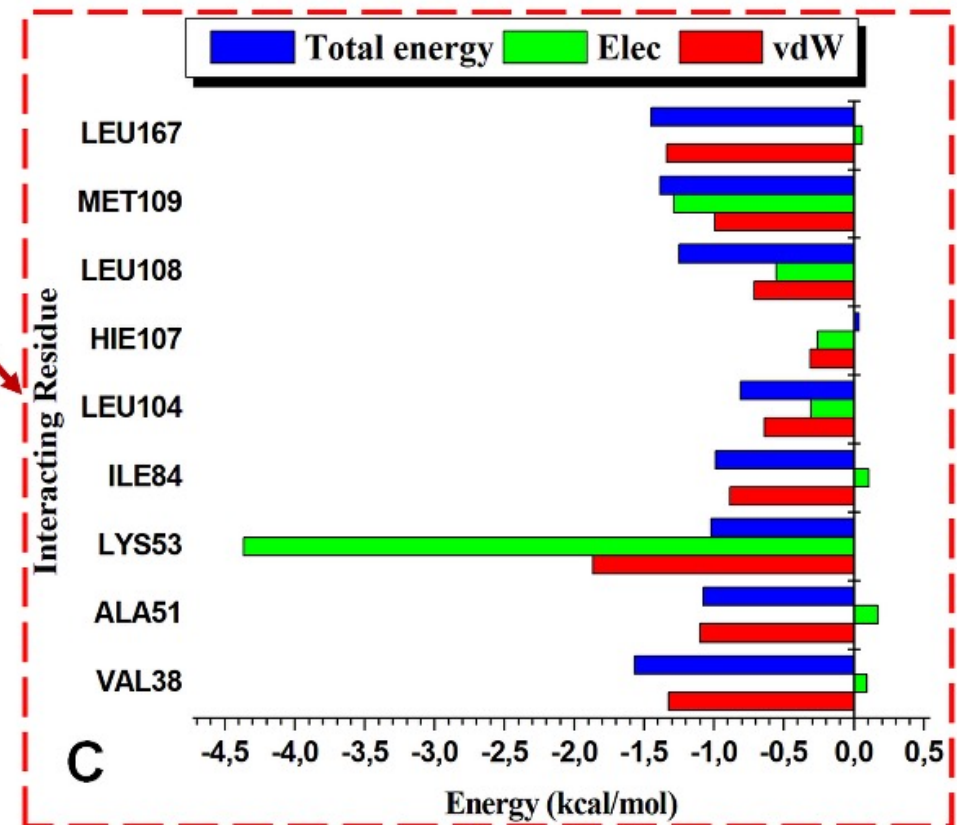
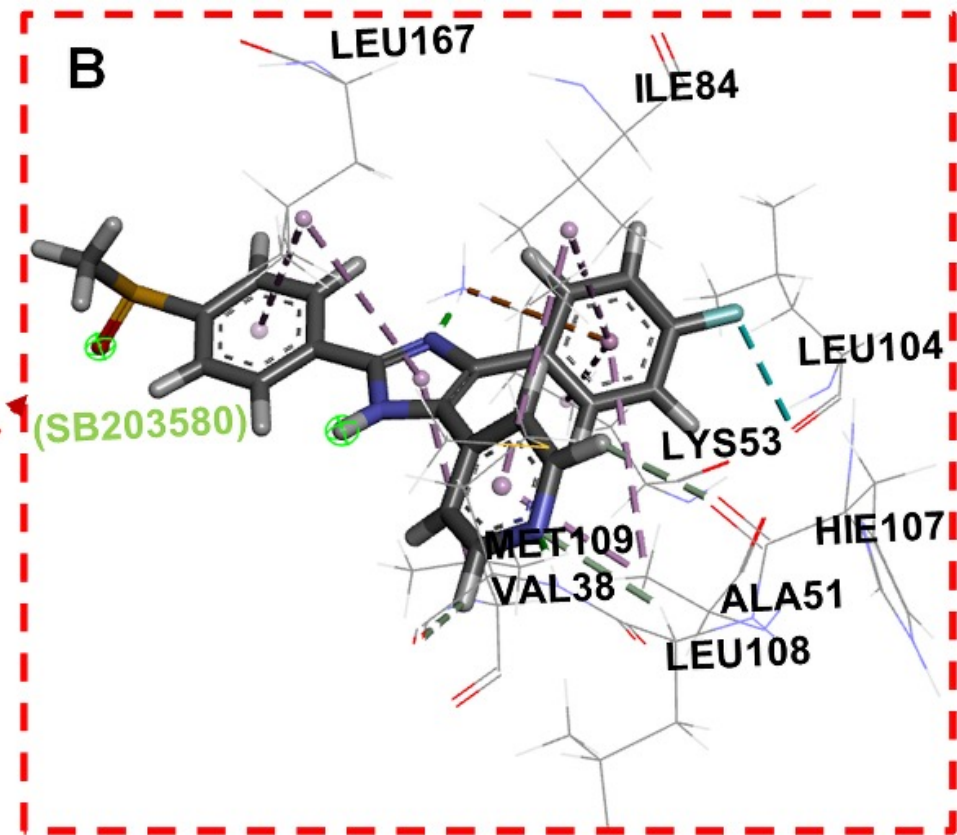
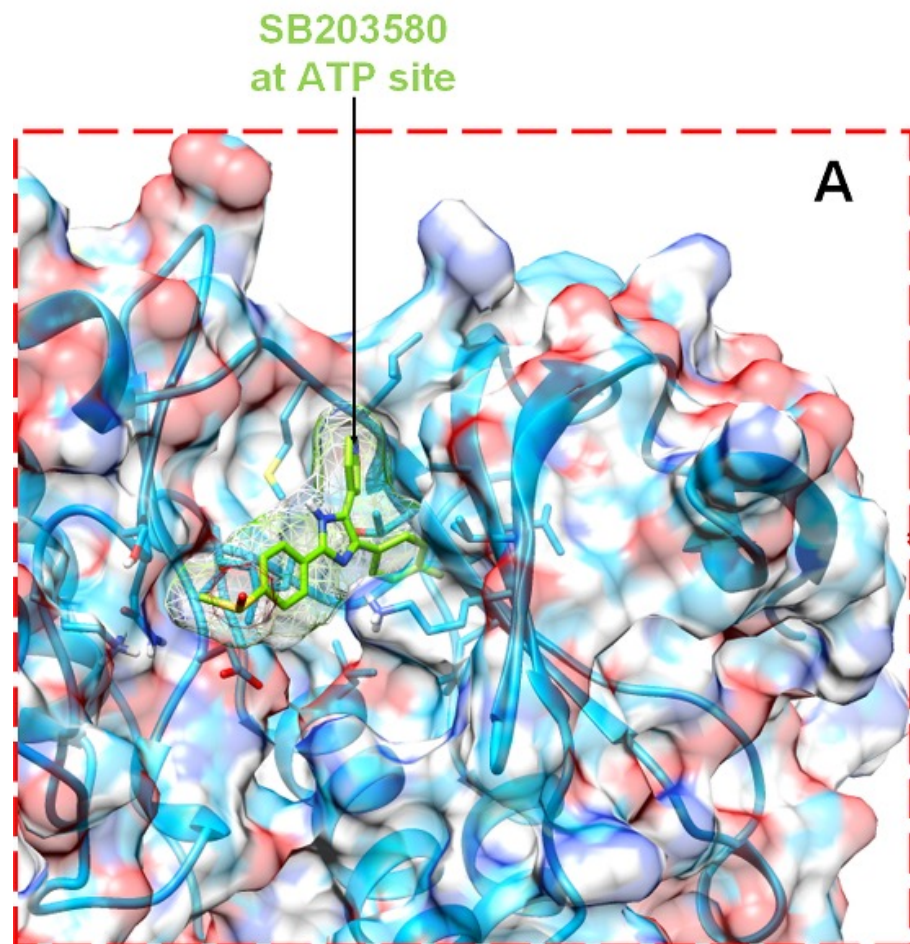


Figure 4

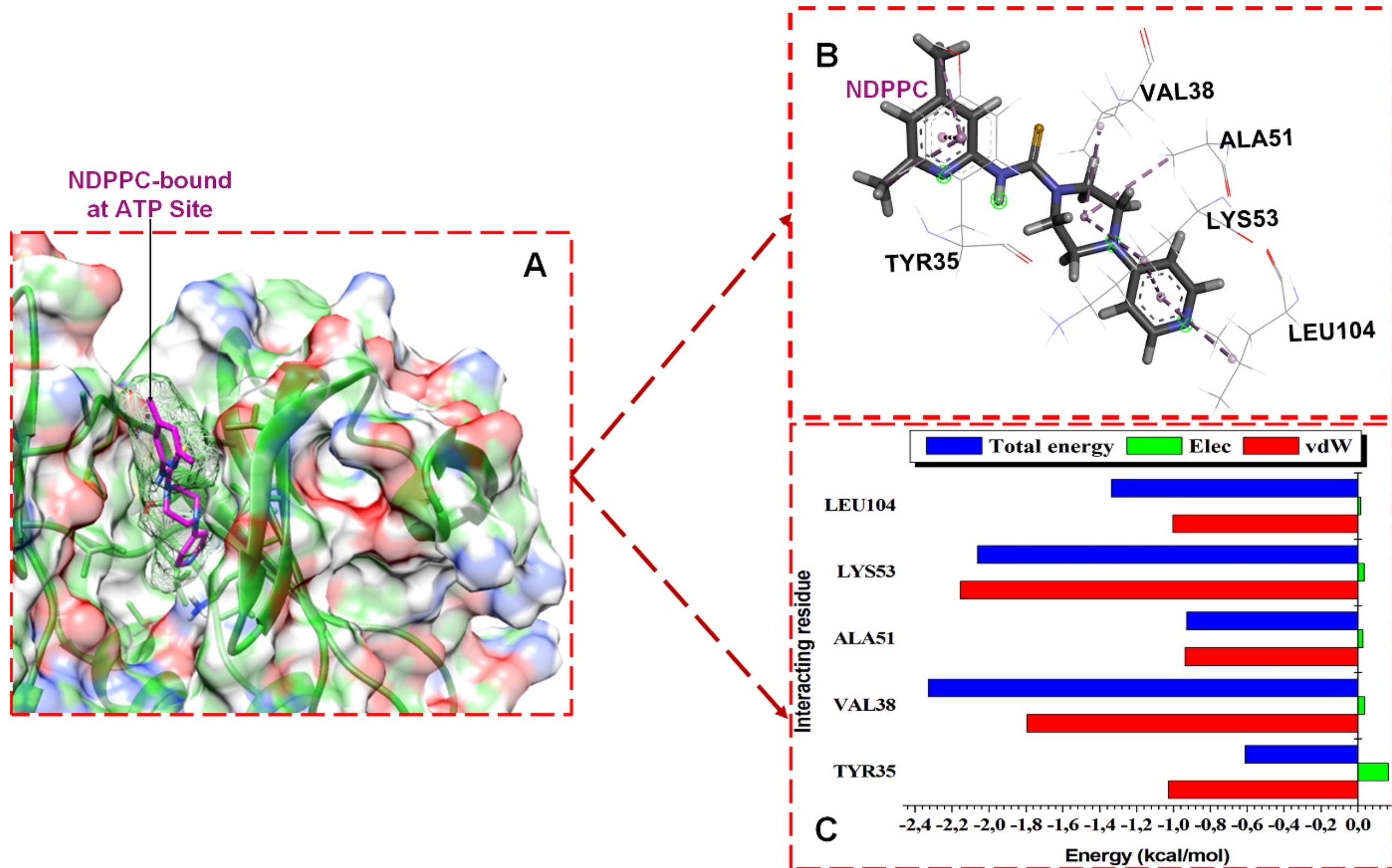


Figure 5

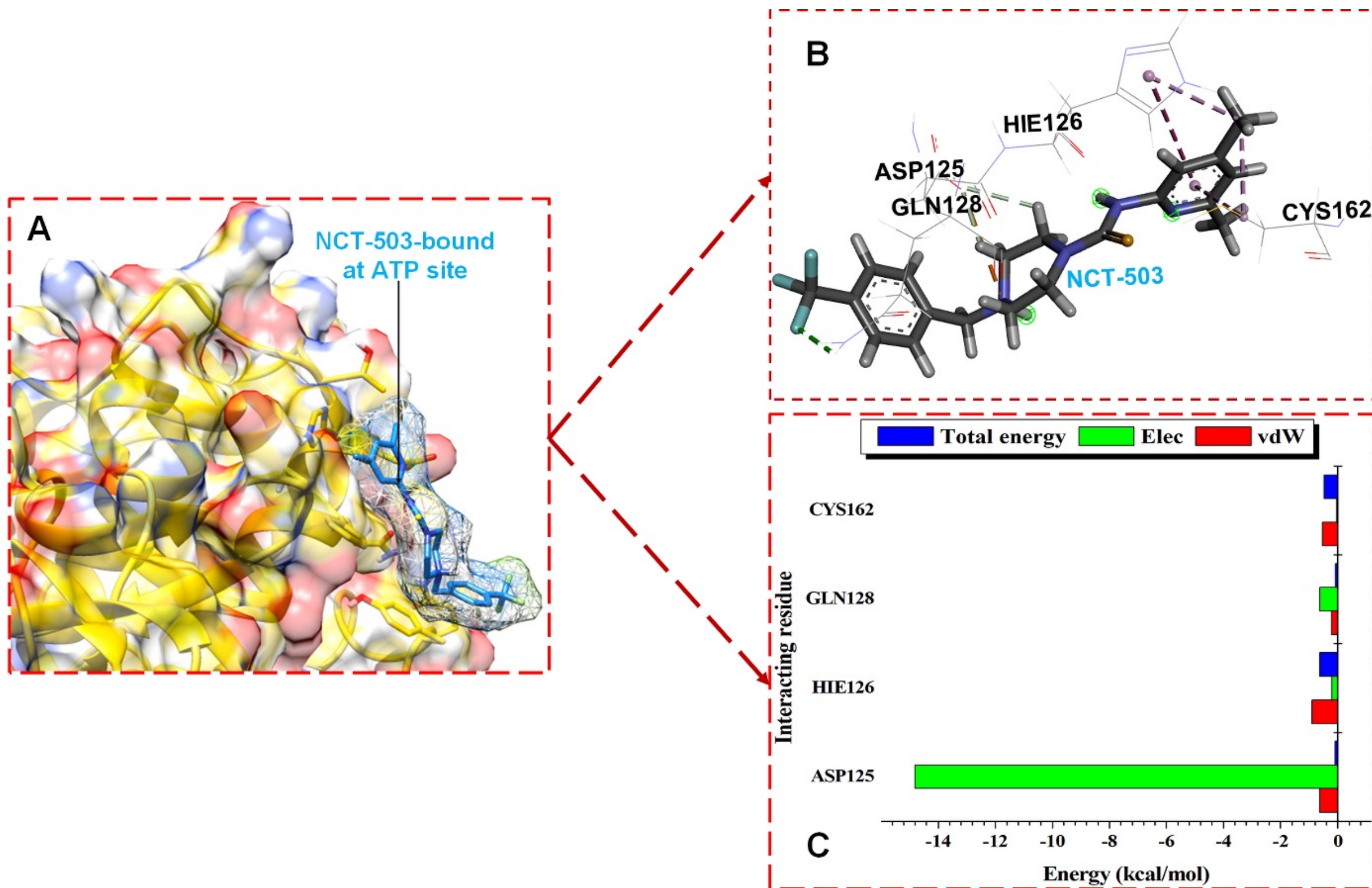


Figure 6

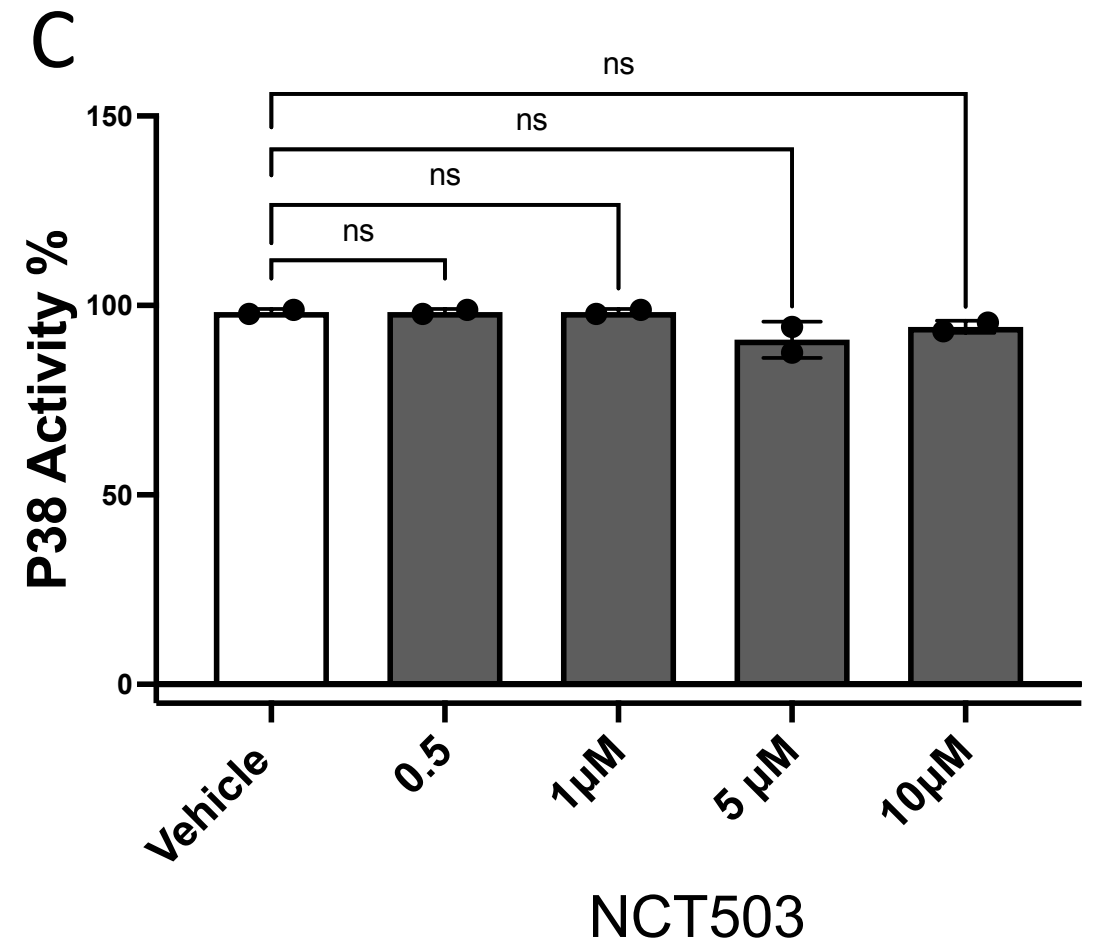
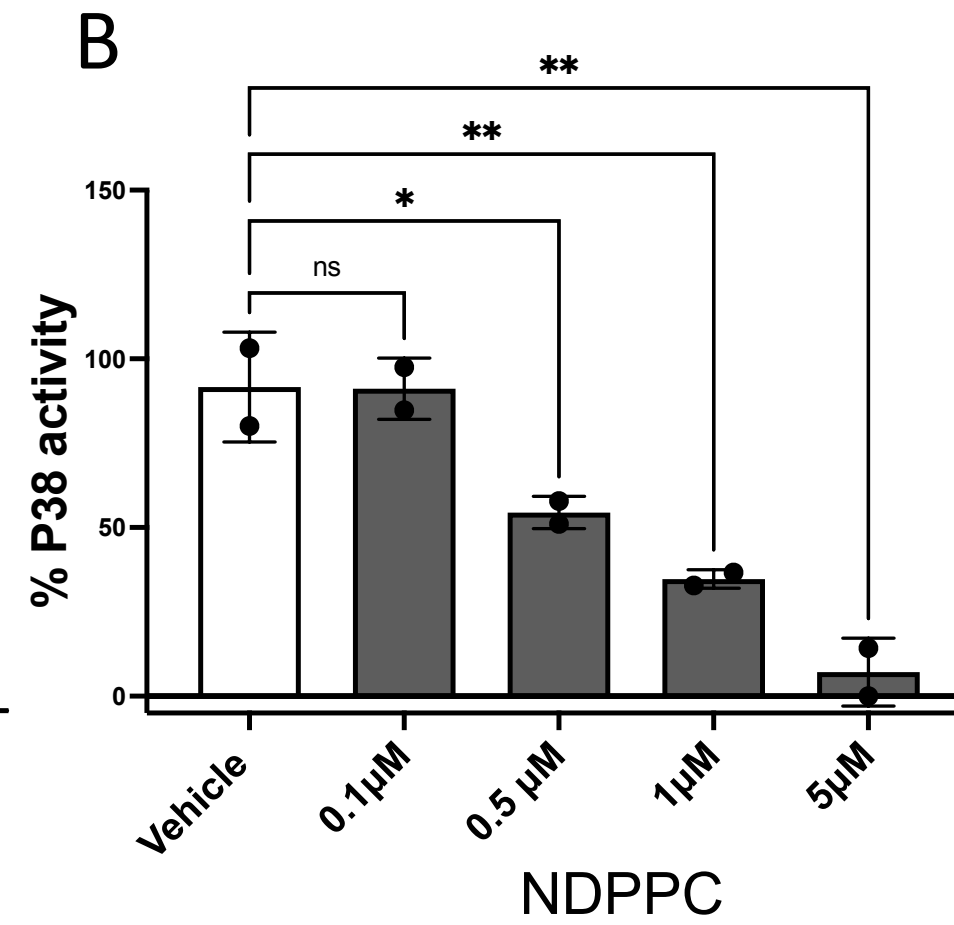
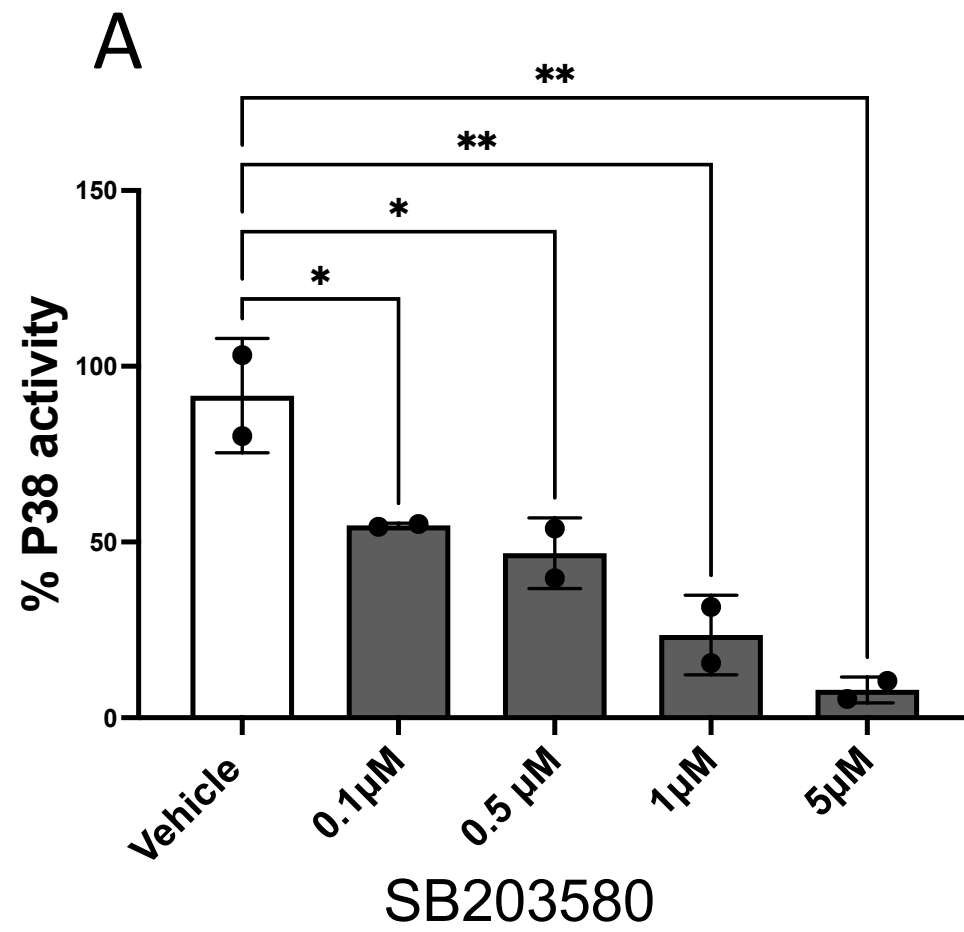
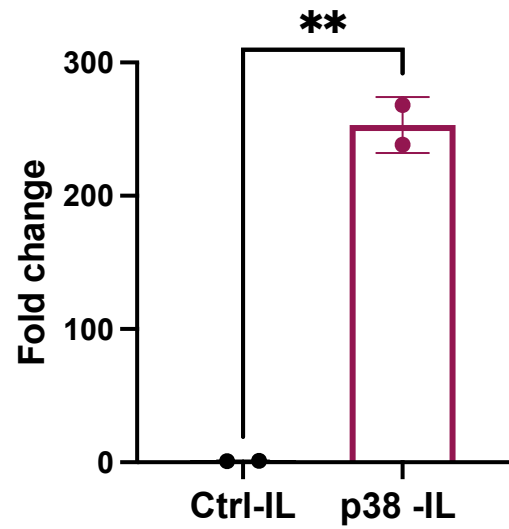
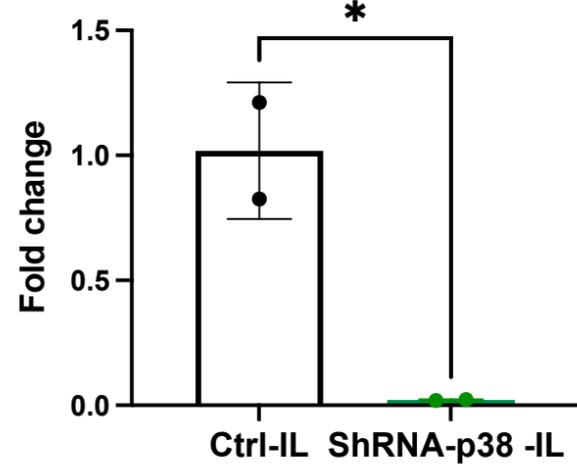


Figure 7

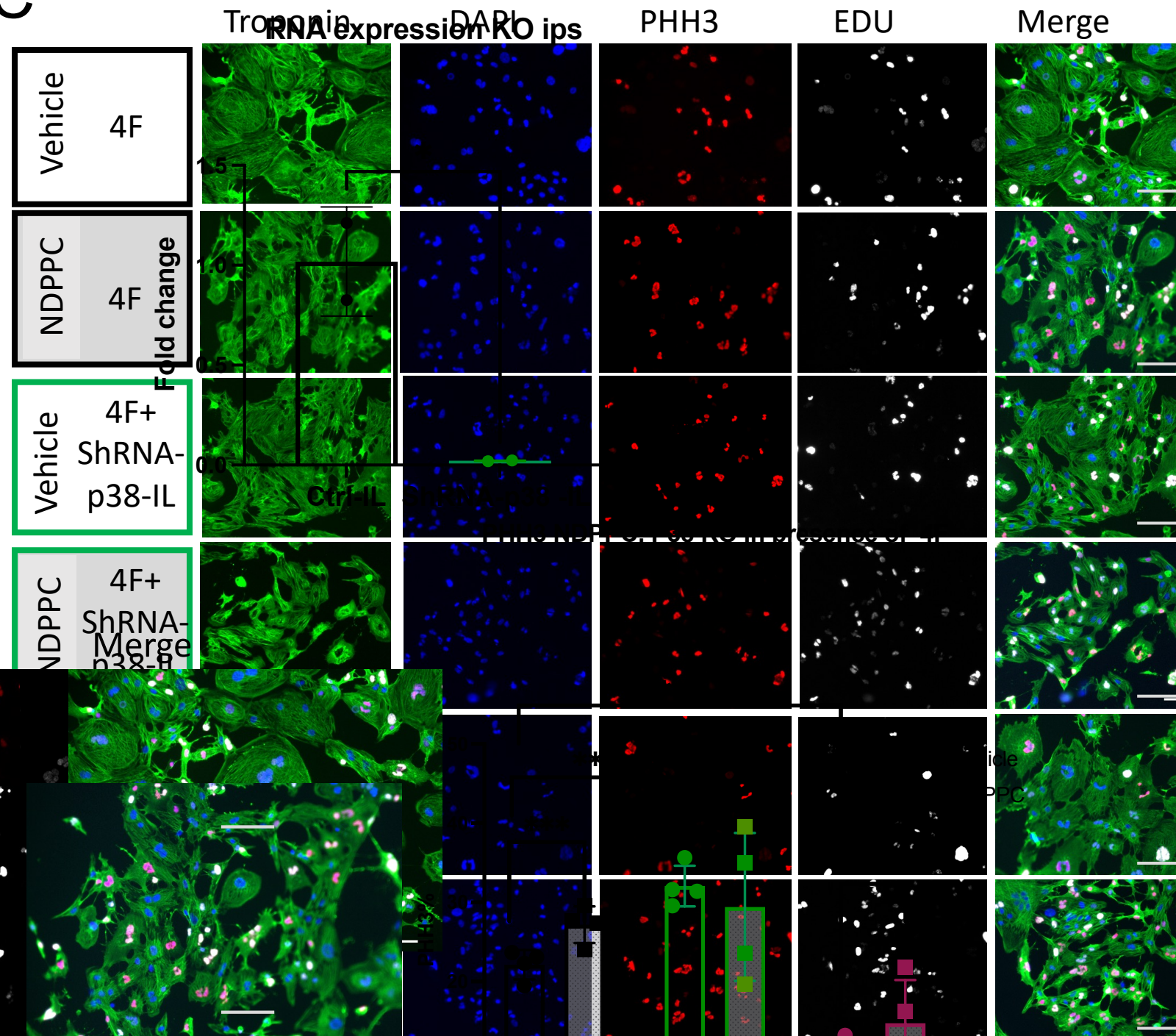
A



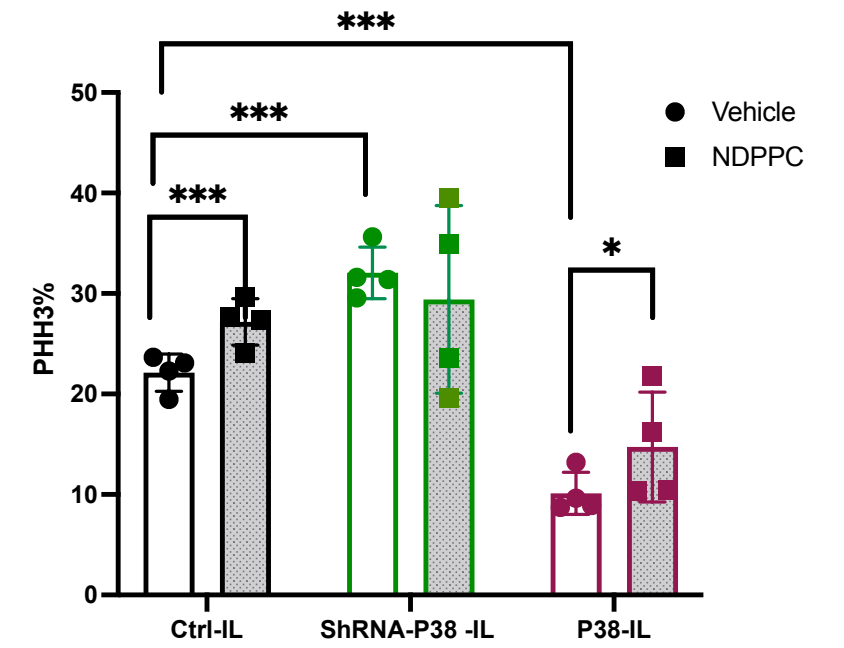
B



C



D



E

